Molecular Therapy
Nucleic Acids
Original Article

The Chromatin Structure of CRISPR-Cas9 Target DNA Controls the Balance between Mutagenic and Homology-Directed Gene-Editing Events

Josephine M. Janssen,[1,2] Xiaoyu Chen,[1,2,3] Jin Liu,[1] and Manuel A.F.V. Gonçalves[1]

[1]Department of Cell and Chemical Biology, Leiden University Medical Center, Einthovenweg 20, 2333 ZC Leiden, the Netherlands

Gene editing based on homology-directed repair (HDR) depends on donor DNA templates and programmable nucleases, e.g., RNA-guided CRISPR-Cas9 nucleases. However, next to inducing HDR involving the mending of chromosomal double-stranded breaks (DSBs) with donor DNA substrates, programmable nucleases also yield gene disruptions, triggered by competing non-homologous end joining (NHEJ) pathways. It is, therefore, imperative to identify parameters underlying the relationship between these two outcomes in the context of HDR-based gene editing. Here we implemented quantitative cellular systems, based on epigenetically regulated isogenic target sequences and donor DNA of viral, non-viral, and synthetic origins, to investigate gene-editing outcomes resulting from the interaction between different chromatin conformations and donor DNA structures. We report that, despite a significantly higher prevalence of NHEJ-derived events at euchromatin over Krüppel-associated box (KRAB)-impinged heterochromatin, HDR frequencies are instead generally less impacted by these alternative chromatin conformations. Hence, HDR increases in relation to NHEJ when open euchromatic target sequences acquire a closed heterochromatic state, with donor DNA structures determining, to some extent, the degree of this relative increase in HDR events at heterochromatin. Finally, restricting nuclease activity to HDR-permissive G2 and S phases of the cell cycle through a Cas9-Geminin construct yields lower, hence more favorable, NHEJ to HDR ratios, independently of the chromatin structure.

INTRODUCTION

Genome editing based on inducing targeted chromosomal double-stranded DNA breaks (DSBs) by programmable nucleases permits altering, in a precise manner, the genetic makeup of eukaryotic cells.[1,2] Normally, homology-directed repair (HDR) is the DSB repair pathway that is exploited for the targeted and precise addition of new genetic information. In this case, exogenous DNA templates sharing sequences identical to chromosomal acceptor sites serve as surrogate HDR substrates for repairing the underlying sequence-specific DSBs. Ultimately, this co-option of HDR yields precise genetic alterations at predefined genomic sequences.[1,2]

Despite its patent usefulness, HDR-based gene editing is limited by the fact that, in mammalian cells, DSBs are primarily repaired through competing non-homologous end joining (NHEJ) pathways instead of through HDR.[3,4] Moreover, HDR is commonly restricted to the G2-S phases of the cell cycle, when sister chromatid sequences become available, while NHEJ, involving end-to-end ligation of broken chromosomal termini, takes place throughout the various stages of the cell cycle.[3,4] Critically, NHEJ-mediated DSB repair leads to chromosomal translocations and, more often, to the incorporation of small insertions and deletions (indels) at the target site, resulting in disruptive, potentially deleterious, allelic mutations. Hence, it is crucial to expand our knowledge about the parameters governing these two DNA repair pathway-driven gene editing endpoints that, together, determine the performance of HDR-based gene editing and genomic DNA stability.

Chromatin is formed in the nucleus of eukaryotic cells by a dynamic association between genomic DNA and various types of molecules, including histones and non-histone proteins. The basic unit of chromatin, the nucleosome, consists of ~147 bp of double helix wrapped around an octamer of the four core histones H3, H4, H2A, and H2B.[5] The transition from compact or closed heterochromatin to relaxed or open euchromatin is controlled through a large number of macromolecular complexes and their respective catalytic activities, which include methylation-demethylation, acetylation-deacetylation, and phosphorylation-dephosphorylation.[5] The impact of different chromatin states on programmable nuclease-assisted gene editing at on-target sequences, as well as on the genome-wide distribution of off-target sites, warrants in-depth investigations.[6]

Our laboratory and those of others have reported that NHEJ-mediated repair of a single DSB induced by programmable nucleases can be modulated by distinct epigenetic marks and chromatin structures in living mammalian cells.[7–14] As of yet, however, the role played by

Received 25 June 2018; accepted 11 February 2019;
https://doi.org/10.1016/j.omtn.2019.02.009.

[2]These authors contributed equally to this work.

[3]Present address: Department of Psychiatry and Behavioral Sciences, Stanford University School of Medicine, Stanford, CA 94305, USA

Correspondence: Manuel A.F.V. Gonçalves, Department of Cell and Chemical Biology, Leiden University Medical Center, Einthovenweg 20, 2333 ZC Leiden, the Netherlands.
E-mail: m.f.v.goncalves@lumc.nl

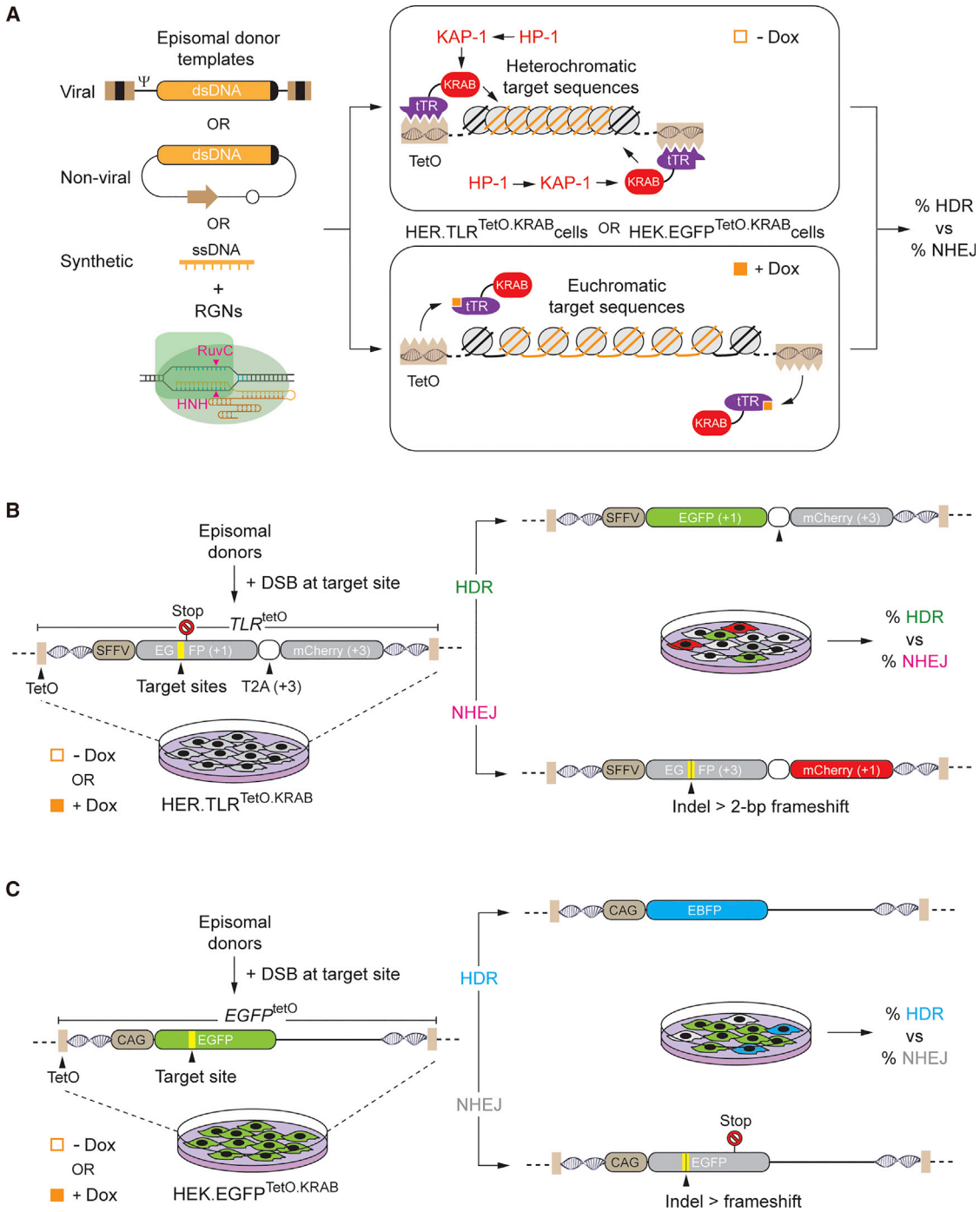

Figure 1. Experimental Systems for Tracking Gene-Editing Outcomes at Isogenic Target Sequences with Alternative Epigenetic States

(A) Generic experimental designs. The reporter HER.TLR$^{TetO.KRAB}$ and HEK.EGFP$^{TetO.KRAB}$ cells, cultured in the absence or presence of Dox, are exposed to RGNs together with different donor DNA templates. Without Dox, tTR-KRAB binds to *TetO* and induces heterochromatin formation through the recruitment of, among other factors, KAP1 and HP1. With Dox, tTR-KRAB is set free from *TetO*, leading the target sequences to acquire an euchromatic state. After the completion of the gene-editing processes, Dox is added to the different cultures in order to determine the frequencies of HDR and NHEJ events at heterochromatic versus euchromatic target sequences by dual-color flow cytometry. (B) *Modus operandi* of the Traffic Light Reporter (TLR)-containing HER.TLR$^{TetO.KRAB}$ indicator cells for tracking gene-editing endpoints at heterochromatin versus euchromatin. The *TetO*-flanked *TLR*^{TetO} construct in tTR-KRAB-expressing HER.TLR$^{TetO.KRAB}$ cells has an *EGFP* open reading frame (ORF) interrupted by heterologous

(legend continued on next page)

such chromosomal topologies on the performance of HDR-based gene editing, using different types of donor DNA templates, has not been assessed. To start addressing this matter, here we sought to investigate whether distinct chromatin conformations, regulated through the recruitment of the Krüppel-associated box (KRAB) domain to DNA, controls gene-editing outcomes by changing the balance between HDR and NHEJ events at single, site-specific DSBs. KRAB-containing proteins belong to the largest family of zinc-finger repressors in tetrapod vertebrates, whose generic role is that of recruiting chromatin remodeling co-repressors via their KRAB domains, after binding to specific genomic sequences through their zinc-finger motifs.[15,16] In particular, KRAB domains interact with KRAB-associated protein-1 (KAP1) oligomers that form a scaffold for the binding of heterochromatin-1 (HP1) isoforms (i.e., HP1α, HP1β, and HP1γ), histone deacetylases (i.e., HDAC1 and HDAC2), the nucleosome-remodeling factor CHD3, and the SET domain histone methyl-transferase SETDB1 that associates with additional HP1 molecules via tri-methylation of lysine 9 on histone H3 (H3K9me3).[15,16] Ultimately, these large protein-DNA assemblies create heterochromatic regions in the genome.[17,18]

Here, to assess the influence of chromatin structure on HDR-based gene editing, we combined (1) human reporter cells with target sequences under the control of KRAB-mediated epigenetic regulation; (2) programmable RNA-guided nucleases (RGNs) based on the type II CRISPR-Cas9 adaptive immune system from *S. pyogenes*;[19] and (3) donor HDR substrates of viral, non-viral, and synthetic origins. In particular, as donors, we tested integrase-defective lentiviral vector genomes (IDLVs),[20] conventional recombinant plasmids, and chemically synthesized single-stranded oligodeoxyribonucleotides (ODNs) with both polarities (i.e., sense and antisense). RGNs are ribonucleoproteins formed by a complex between a fixed Cas9 protein and a sequence-tailored guide RNA (gRNA). Typically, the 5′-terminal 20 nt of the gRNA (spacer) are tailored to hybridize to a chromosomal target sequence located next to a protospacer adjacent motif (PAM; NGG in the case of *S. pyogenes* Cas9). The PAM sequence signals the position for the initial protein-DNA binding mediated through the PAM-interacting domain positioned on the two lobes of Cas9.[21] Next, complementarity between the spacer portion of the gRNA and PAM-adjoined DNA sequences triggers DSB formation by the coordinated catalytic activation of the nuclease domains of Cas9 (i.e., HNH and RuvC).[19]

By using the aforementioned DNA, RNA, and protein tools, we performed gene-editing experiments in quantitative live-cell readout systems, based on complementary human reporter cells containing chromosomal target sequences whose KRAB-regulated epigenetic statuses are controlled by small molecule drug availability.[10,11] We report that the proportions between gene-editing endpoints resulting from the repair of site-specific DSBs by NHEJ and HDR differ in a chromatin structure-dependent manner, with HDR increasing its prominence in relation to NHEJ when euchromatic target sequences acquire a heterochromatic state. Of note, the type of donor DNA can have a measurable impact on the extent to which this relative increase in HDR events takes place at KRAB-induced heterochromatic target sites. Further, we found that a Cas9-Geminin fusion protein, whose activity is downregulated during the HDR non-permissive cell cycle phases,[22] in addition to enhancing HDR rates decreases those of NHEJ, resulting in a net gain of HDR-derived gene-editing events at both euchromatin and KRAB-induced heterochromatin.

RESULTS

Gene-editing experiments were carried out in HER.Traffic Light Reporter (TLR)$^{TetO.KRAB}$ and HEK.EGFP$^{TetO.KRAB}$ cells by introducing RGNs together with donors of viral, non-viral, or synthetic origins (Figure 1). These human reporter cells express the *E. coli* tetracycline trans-repressor (tTR) fused to a mammalian KRAB domain. The tTR and KRAB components are, hence, the DNA-binding and effector domains of the tTR-KRAB fusion product, respectively. In HER.TLR$^{TetO.KRAB}$ and HEK.EGFP$^{TetO.KRAB}$ cells, in the absence of doxycycline (Dox), the tTR-KRAB fusion protein binds to its cognate *TetO* sequences and recruits via its KRAB repressor domain the endogenous epigenetic silencing apparatus, consisting of, among other chromatin-remodeling factors, the co-repressor KAP1 and HP1 (Figure 1A). Conversely, in the presence of Dox, tTR-KRAB suffers a conformational change that releases it from the *TetO* sequences. This results in the transition of associated sequences from a compacted heterochromatic state (H3K9me3 high, H3-Ac low) into a relaxed euchromatic state (H3-Ac high, H3K9me3 low), as shown previously.[10]

We reasoned that the complementary gain-of-function and loss-of-function assays offered by HER.TLR$^{TetO.KRAB}$ and HEK.EGFP$^{TetO.KRAB}$ cells should be particularly suited for assessing the impact of epigenetically regulated chromatin conformations on specific gene-editing endpoints. This is so owing to the fact that these live-cell systems permit the simultaneous quantification of HDR and NHEJ events at isogenic target sequences located either in euchromatin or heterochromatin, depending on the presence or absence of Dox, respectively

sequences and a stop codon located upstream of a T2A sequence and an out-of-frame *mCherry* reporter. HDR is scored by measuring EGFP$^+$ cells resulting from the repair of site-specific DSBs by HR events between episomal donor templates (EGFPtrunc) and heterochromatic (−Dox) or euchromatic (+Dox) chromosomal DNA. This genetic conversion results in the substitution of the heterologous and stop codon DNA by an in-frame *EGFP* sequence. Concomitantly, NHEJ is scored by measuring mCherry$^+$ cells resulting from the fraction of indels placing the *mCherry* in-frame. (C) *Modus operandi* of HEK.EGFP$^{TetO.KRAB}$ indicator cells for tracking gene-editing endpoints at heterochromatin versus euchromatin. The *TetO*-flanked *EGFP* construct (*EGFP*^{TetO}) in tTR-KRAB-expressing HEK.EGFP$^{TetO.KRAB}$ cells is functional. HDR is tracked by measuring the frequencies of blue light-emitting cells resulting from the conversion of the *EGFP* fluorochrome into that of *EBFP*. Simultaneously, NHEJ is scored by measuring EGFP$^-$ cells resulting from indels placing the *EGFP* sequence out-of-frame. The RGN complexes delivered into HEK.EGFP$^{TetO.KRAB}$ cells cleave within the EGFP fluorochrome-coding region. As a result, the vast majority of DSB-derived indels are expected to yield EGFP-negative cells.

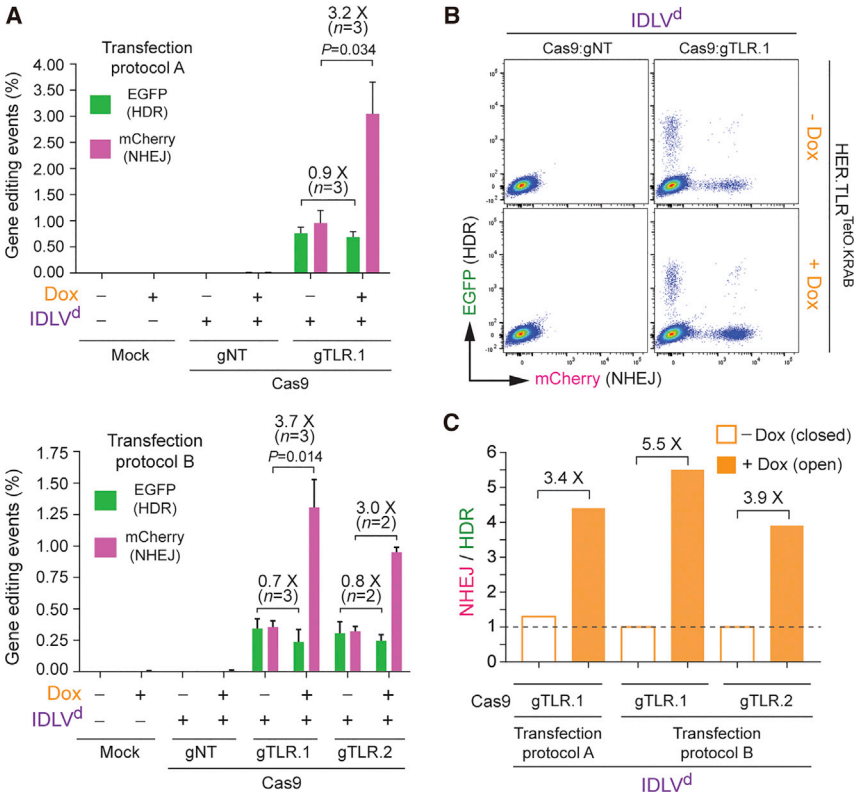

Figure 2. Comparing Gene-Editing Outcomes at Euchromatin versus Heterochromatin after Viral Vector Delivery of Donor DNA

(A) IDLV^{d}-based gene editing. Dual-color flow cytometric measurements of HDR and NHEJ frequencies in HER.TLR$^{TetO.KRAB}$ cells subjected to the indicated experimental conditions and treated (+) or not treated (–) with Dox are shown. Two different transfection protocols (A and B) were used to introduce the DNA constructs into target cells. IDLV^{d} particles were applied at an MOI of 8 VP cell^{-1}. Bars correspond to mean ± SD of the indicated number (n) of independent experiments (biological replicates done on different days). (B) Representative dot plots corresponding to HER.TLR$^{TetO.KRAB}$ cells exposed to IDLV^{d} together with Cas9:gNT or Cas9:gTLR.1 complexes initially treated or not treated with Dox. (C) Comparative engagement of HDR and NHEJ pathways during IDLV-mediated repair of DSBs made at heterochromatin versus euchromatin. Panel C presents the data shown in (A) as the ratios between the rates of NHEJ and HDR in HER.TLR$^{TetO.KRAB}$ cells incubated or not incubated with Dox.

(Figure 1A). Indeed, in these cells, Dox availability regulates the tTR-KRAB-mediated recruitment of the aforementioned endogenous chromatin-remodeling complexes to *TetO* sequences associated with each of the reporter alleles, i.e., *TLR*^{TetO} and *EGFP*^{TetO} (Figures 1B and 1C).

HDR-based gene editing experiments were started by transfecting HER.TLR$^{TetO.KRAB}$ cells, cultured in the absence or in the presence of Dox, with plasmids encoding the RGN complex Cas9:gTLR.1. The target site of Cas9:gTLR.1 is located upstream of a nonsense mutation within the *TLR*^{TetO} construct, and it is flanked by sequences homologous to those present in the *EGFP*-repairing donor template EGFPtrunc[23] (Figure 1B; Figure S1). This HDR substrate was delivered by transducing HER.TLR$^{TetO.KRAB}$ cells with different amounts of the integrase-defective lentiviral vector IDLV^{d} together with constructs expressing the RGN complex Cas9:gTLR.1 (Figure S2). Negative controls consisted of HER.TLR$^{TetO.KRAB}$ cells that received neither expression plasmids nor IDLV^{d} particles (mock), and they were exposed to an irrelevant, non-targeting, gRNA (gNT) together with Cas9 and IDLV^{d}. After the action of the RGN complexes had taken place, all HER.TLR$^{TetO.KRAB}$ cultures were incubated in the presence of Dox for allowing transgene expression and quantification of HDR- and NHEJ-derived gene editing events by EGFP- and mCherry-directed flow cytometry, respectively. The IDLV^{d} dose-response treatments revealed that the HDR levels plateaued with an MOI of 8 vector particles per cell (VP cell^{-1}) (Figures S2A and S2B). Thus, this dose of IDLV^{d} particles was chosen for subsequent transduction experiments.

We found that the frequencies of DSB-triggered NHEJ at euchromatic target sequences (+Dox) were substantially higher than those measured at their heterochromatic (−Dox) counterparts, as assessed by mCherry-directed flow cytometry (Figures 2A and 2B). This outcome is in agreement with that of our previous study involving the exclusive delivery of RGNs.[10] In particular, RGN-induced DSBs are preferentially formed at euchromatin over heterochromatin,[10] which, in turn, directly correlates with the preferential binding of RGNs harboring catalytically inert (dead) Cas9 proteins to euchromatic over heterochromatic regions across the genome, as determined by chromatin immunoprecipitation sequencing (ChIP-seq) analysis.[24–26] Interestingly, despite an initial higher accessibility of gene-editing tools to euchromatic over heterochromatic DNA, there were no corresponding increases in HDR levels in the former, Dox-treated cells (Figure 2A). As a result, the ratios between NHEJ and HDR events at compact heterochromatin were substantially lower, and hence more favorable, than those measured at relaxed euchromatin (Figure 2C; Figure S2C). The use of the alternative RGN complex Cas9:gTLR.2 recapitulated the outcome obtained with Cas9:gTLR.1 (Figures 2A, lower panel, and 2C).

Next, we sought to assess RGN-induced gene-editing endpoints at isogenic target sequences with distinct chromatin conformations, after delivering donor DNA in the context of covalently closed double-stranded plasmids. In these experiments, we deployed the lentiviral DNA construct Plasmid^{d},[23] which had been utilized for assembling IDLV^{d} particles. These experiments involved transfecting donor Plasmid^{d} mixed with constructs expressing Cas9:gTLR.1, Cas9:gTLR.2,

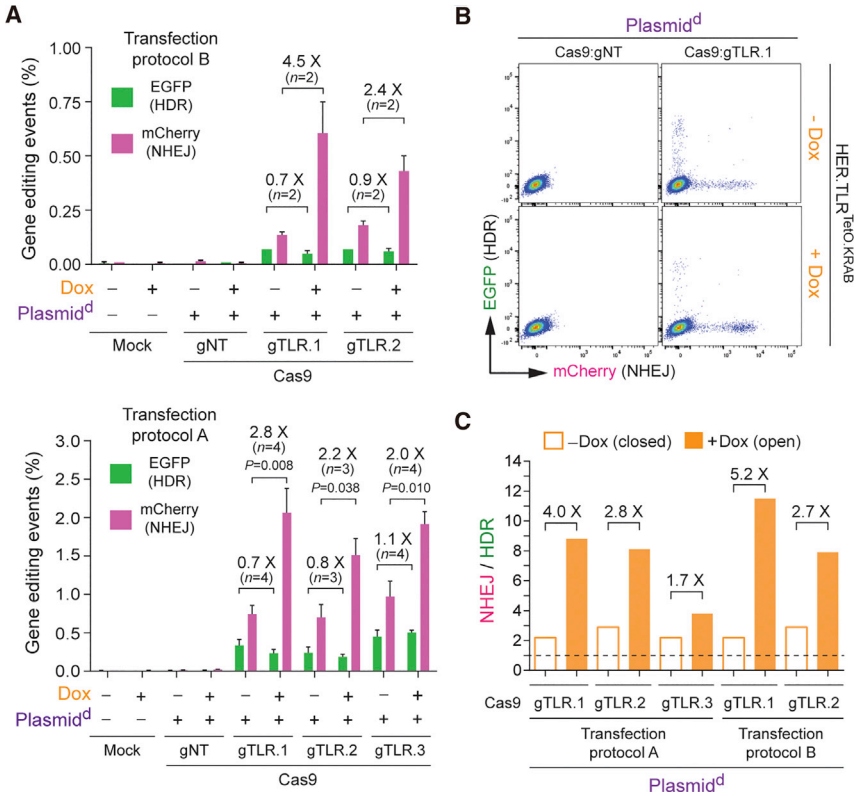

Figure 3. Comparing Gene-Editing Outcomes at Euchromatin versus Heterochromatin after Plasmid Vector Delivery of Donor DNA

(A) Plasmid[d]-based gene editing. Dual-color flow cytometric quantification of HDR and NHEJ frequencies in HER.TLR[TetO.KRAB] cells are shown. HER.TLR[TetO.KRAB] cells incubated (+) or not incubated (–) with Dox were mock-transfected or were transfected with Plasmid[d] mixed with constructs encoding the indicated RGN complexes. Two different transfection protocols (A and B) were used to deliver the DNA constructs into target cells. Bars represent mean ± SD of the indicated number (n) of independent experiments (biological replicates done on different days). (B) Representative dot plots corresponding to HER.TLR[TetO.KRAB] cells transfected with Plasmid[d] mixed with expression constructs coding for Cas9:gNT or Cas9:TLR.1 complexes initially treated or not treated with Dox. (C) Relative engagement of HDR and NHEJ pathways during plasmid-mediated repair of DSBs created at heterochromatin versus euchromatin. Panel C displays the data shown in (A) as the ratios between the frequencies of NHEJ and HDR in HER.TLR[TetO.KRAB] cells exposed or not exposed to Dox.

or Cas9:gTLR.3 complex (Figure S1) into HER.TLR[TetO.KRAB] cells treated or not treated with Dox. The resulting gene-editing outcomes were similar to those obtained after IDLV[d] transduction of HER.TLR[TetO.KRAB] cells. In particular, the frequencies of HDR were similar at heterochromatin and euchromatin, whereas the frequencies of NHEJ were clearly higher at euchromatic target DNA (Figures 3A and 3B). Interestingly, plasmid donors led to a less balanced participation of NHEJ and HDR in the repair of heterochromatic DSBs (Figure 3C; NHEJ to HDR ratios > 1), when compared to that resulting from using IDLV donors (Figure 2C). As a corollary, these data indicate that the type and/or structure of the DSB-repairing HDR substrates can influence the ultimate performance of gene-editing procedures. Notwithstanding the above, in comparison with euchromatin, at heterochromatin established by the KRAB-KAP1-HP1-remodeling axis, the balance between NHEJ and HDR shifted toward the latter DNA repair pathway, causing target cell populations to acquire a more even, and hence more favorable, distribution between HDR- and NHEJ-derived genetic modifications (Figure 3C).

To serve as additional controls, gene-editing experiments were also performed in tTR-KRAB-expressing HER.TLR[KRAB] cells whose target sequences were not under conditional KRAB-mediated epigenetic regulation due to their lack of the *TetO cis*-acting elements necessary for tTR-KRAB binding (Figure 4A). Importantly, regardless of the Dox regimen, neither the HDR levels nor the NHEJ levels changed in HER.TLR[KRAB] cells, independently of whether the donor DNA was introduced into target cell nuclei in the context of linear IDLV[d] genomes (Figure 4B) or covalently closed Plasmid[d] molecules (Figure 4C). Hence, in contrast to gene-editing experiments in HER.TLR[TetO.KRAB] cells, in control HER.TLR[KRAB] cells, there were no substantial Dox-dependent variations in the proportions between HDR and NHEJ events for both types of donor DNA templates used (Figure 4D).

To provide for an independent experimental system, we also performed gene-editing experiments in HEK.EGFP[TetO.KRAB] cells. In this system, HDR can be promptly tracked by measuring cells in which the EGFP fluorochrome is converted into that of EBFP after donor DNA delivery, while NHEJ can be monitored through quantifying cells in which nuclease-induced indels yield *EGFP* knockouts (Figures 1C, 5A, and 5B). HEK.EGFP[TetO.KRAB] cells, cultured in the absence or presence of Dox, were transfected with plasmid pTHG.Donor together with constructs encoding the Cas9:gEGFP complex targeting the EGFP fluorochrome-coding sequence (Figure 5A). The results were in agreement with those obtained in HER.TLR[TetO.KRAB] cells (Figures 2 and 3) in that, notwithstanding the higher frequencies of NHEJ events measured at euchromatin over those measured at heterochromatin, HDR levels were more comparable at both chromatin states (Figure 5C). As a result, the ratios between NHEJ and HDR events at heterochromatin were consistently lower than those measured at euchromatin (Figure 5D).

Normally, in somatic mammalian cells, G1 is by far the longest phase of the cell cycle during which regular cell and organelle biosynthetic activities take place. Associated with this, there is a global increase in histone acetylation and transcriptional activation,[27] potentially

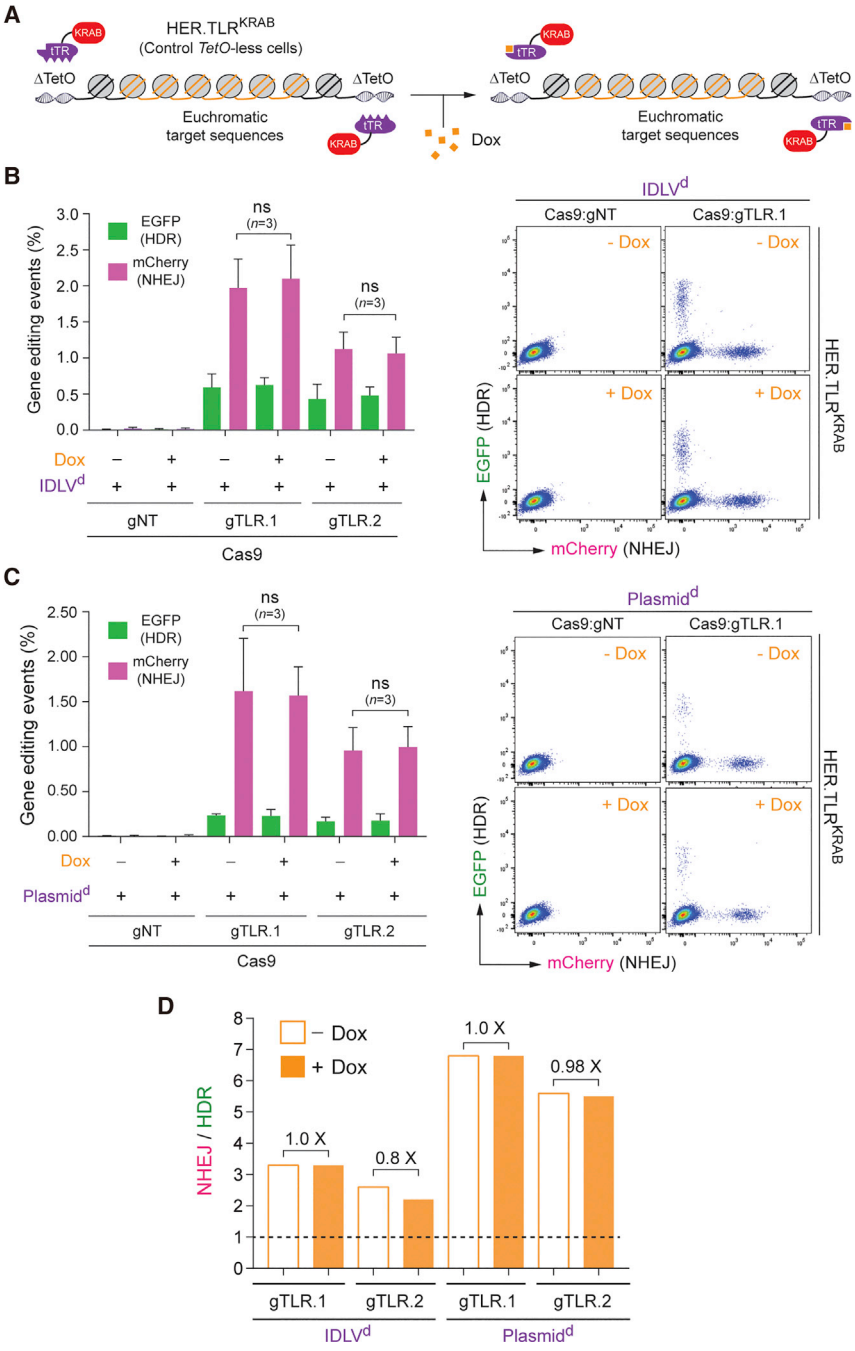

Figure 4. Gene-Editing Endpoints in Control HER.TLR^{KRAB} Cells Exposed or Not Exposed to Dox

(A) Schematics of target DNA in HER.TLR^{KRAB} cells. The tTR-KRAB-expressing HER.TLR^{KRAB} cells have a Dox-insensitive *TLR* construct due to its lack of *cis*-acting *TetO* elements. (B) Dual-color flow cytometric quantification of HDR and NHEJ events in IDLV^{d}-transduced HER.TLR^{KRAB} cells. HER.TLR^{KRAB} cells, treated (+) or not treated (–) with Dox, were exposed to the indicated experimental conditions. IDLV^{d} particles were applied at an MOI of 8 VP cell^{-1}. Right panel: representative dot plots corresponding to HER.TLR^{KRAB} cells exposed to IDLV^{d} particles together with Cas9:gNT or Cas9:TLR.1 complexes. Bars represent mean ± SD of the indicated number (n) of independent experiments (biological replicates done on different days); ns, non-significant. (C) Dual-color flow cytometric quantification of HDR and NHEJ frequencies in Plasmid^{d}-transfected HER.TLR^{KRAB} cells. HER.TLR^{KRAB} cells, incubated (+) or not incubated (–) with Dox, were mock-transfected or were transfected with Plasmid^{d} mixed with constructs encoding the indicated RGN complexes. Right panel: representative dot plots corresponding to HER.TLR^{KRAB} cells transfected with Plasmid^{d} mixed with expression constructs coding for Cas9:gNT or Cas9:TLR.1 complexes. Bars represent mean ± SD of the indicated number (n) of independent experiments (biological replicates done on different days); ns, non-significant. (D) Comparative engagement of HDR and NHEJ pathways at site-specific DSBs created at heterochromatin versus euchromatin. Panel D shows the data presented in (B) and (C) as the ratios between the rates of NHEJ and HDR in HER.TLR^{KRAB} cells not incubated or incubated with Dox.

exposing large regions of the genome to unwarranted programmable nuclease-induced NHEJ during G1. The activity of the APC-Cdh1 E3 ubiquitin ligase complex is high at the late M and G1 phases of the cell cycle, timely triggering ubiquitination and ensuing proteasomal degradation of target proteins.[28] Research has shown that linking Cas9 to a previously identified 110-amino acid sequence of human Geminin,[28] an APC-Cdh1 target protein, results in proteolysis of the Cas9$^{hGem(1/110)}$ fusion product during the HDR non-permissive G1 phase of the cell cycle (Figure 6A).[22] Importantly, when compared to native Cas9, Cas9$^{hGem(1/110)}$ led to a 1.28- to 1.87-fold enhancement of HDR rates in HEK293T reporter cells transfected with an EGFP donor plasmid.[22]

Profiting from the simultaneous tracking of HDR and NHEJ events offered by HER.TLR$^{TetO.KRAB}$ and HER.TLR^{KRAB} cells, we asked whether, in addition to enhancing HDR rates, Cas9$^{hGem(1/110)}$ could improve the balance between HDR and NHEJ events at isogenic sequences regulated by the endogenous KAP1-HP1-dependent chromatin-remodeling apparatus. To this end, HER.TLR$^{TetO.KRAB}$ cells and control HER.TLR^{KRAB} cells, incubated in the presence or absence of Dox, were transfected with plasmids expressing either Cas9 or Cas9$^{hGem(1/110)}$ (Figure 6B), each mixed with constructs encoding four different gRNAs, i.e., gTLR.1, gTLR2, gTLR3, and, as a negative control, gNT. In addition, all transfection reactions included Plasmid^{d} as the source of DSB-repairing templates. Dual-color flow cytometry quantification revealed that, when compared to unmodified Cas9, Cas9$^{hGem(1/110)}$ next to yielding higher frequencies

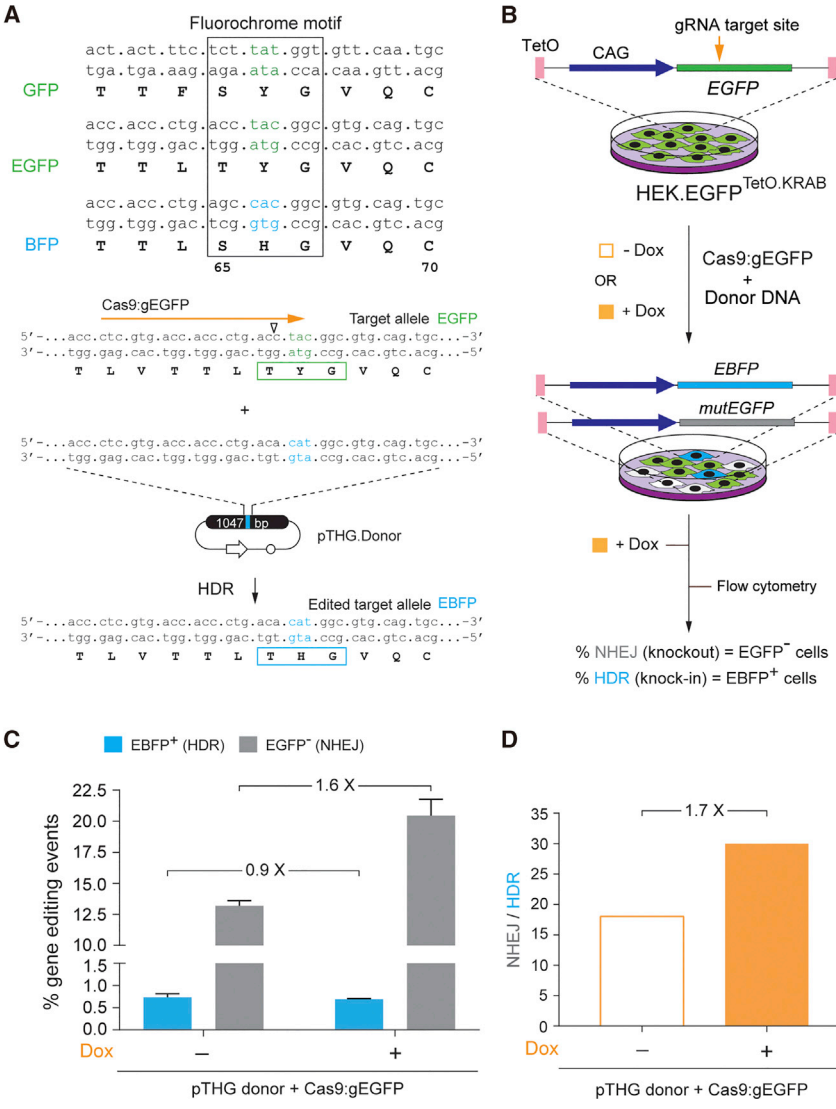

Figure 5. Gene-Editing Outcomes at Euchromatin versus Heterochromatin after Plasmid Donor Delivery into HEK.EGFP$^{TetO.KRAB}$ Cells

(A) Gene-editing assay based on EGFP-to-EBFP fluorochrome conversion. Top panel: nucleic acid and amino acid sequences corresponding to the fluorochromes of GFP, EGFP, and BFP (boxed). Bottom panel: nucleotide and amino acid sequences of the reporter target allele, before and after its editing through the delivery of pTHG.Donor and expression constructs encoding the RGN complex Cas9:gRNA^{EGFP}, are shown. Horizontal orange arrow, target site of Cas9:gRNA^{EGFP}; vertical open arrowhead, position of the DSB induced by Cas9:gRNA^{EGFP}. (B) Schematics of the experimental design applied to HEK.EGFP$^{TetO.KRAB}$ cells. (C) Flow cytometric quantification of HDR and NHEJ frequencies. HEK.EGFP$^{TetO.KRAB}$ cells, incubated (+) or not incubated (–) with Dox, were exposed to pTHG.Donor and gRNA^{EGFP}-containing RGNs. The frequencies of HDR and NHEJ events in the transfected cell populations were determined by measuring EBFP^{+} and EGFP^{-} cells, respectively. Bars indicate mean ± SD of two independent experiments (biological replicates done on different days). (D) Relative participation of HDR and NHEJ pathways during plasmid-mediated repair of DSBs made at heterochromatin versus euchromatin. Panel D presents the data shown in (C) as the ratios between the frequencies of NHEJ and HDR in HEK.EGFP$^{TetO.KRAB}$ cells treated or not treated with Dox.

of HDR led to lower frequencies of NHEJ. This was so regardless of the epigenetic context of target sequences (Figures 6C and 6D). This resulted in a significant net reduction in the ratios between NHEJ- and HDR-derived gene editing events (Figures 6E and 6F), with the most even participation of both DNA repair pathways observed after introducing Cas9$^{hGem(1/110)}$ into cells containing heterochromatic target sequences (Figure 6E; −Dox, solid bars).

Finally, to complement the previous experiments testing linear and covalently closed double-stranded donors in the form of IDLVs and recombinant plasmids, respectively, we sought to assess ODN-based gene editing at euchromatin versus heterochromatin. For these experiments, we selected a single-stranded ODN pair corresponding to the sense and antisense polarities of the target polynucleotide chains of Cas9:gEGFP (i.e., ODN.s and ODN.as, respectively) (Figure 7A). Previous research has demonstrated that RGNs can display a long residence time on target DNA (~6 h) and that, after DNA cutting, the strand upstream of the PAM (non-target strand) is released from the Cas9-gRNA-DNA ternary complex, forming a 3′-ended DNA flap.[29] This insight permitted the design of optimized single-stranded ODN donors whose main attribute consisted of their hybridization to the released strand, i.e., flap (Figure 7A). When compared to double-stranded ODNs and to single-stranded ODNs that cannot anneal to RGN-generated flaps, ODNs complementary to the released strand induced ~4-fold and ~2-fold higher frequencies of HDR in reporter cells, respectively.[29]

Results from an initial experiment in HEK.EGFP$^{TetO.KRAB}$ cells exposed to Cas9:gEGFP together with ODN.s or ODN.as were consistent with the aforementioned data in that the flap-hybridizing ODN.as yielded ~2-fold higher frequencies of HDR than the non-hybridizing ODN.s (Figure 7B). In addition, expanding these ODN transfection experiments to HEK.EGFP$^{TetO.KRAB}$ cells treated or not treated with Dox revealed that, at both chromatin states, i.e., euchromatin (+Dox) and heterochromatin (−Dox), the flap-hybridizing donor ODN.as consistently yielded a more even distribution between HDR and NHEJ events when compared to its ODN.s counterpart (Figure S3). Thus, in addition to their improved HDR proficiency,[29] these results provide a further rationale for selecting single-stranded ODNs whose sequence is complementary to that of the RGN-released DNA flap.

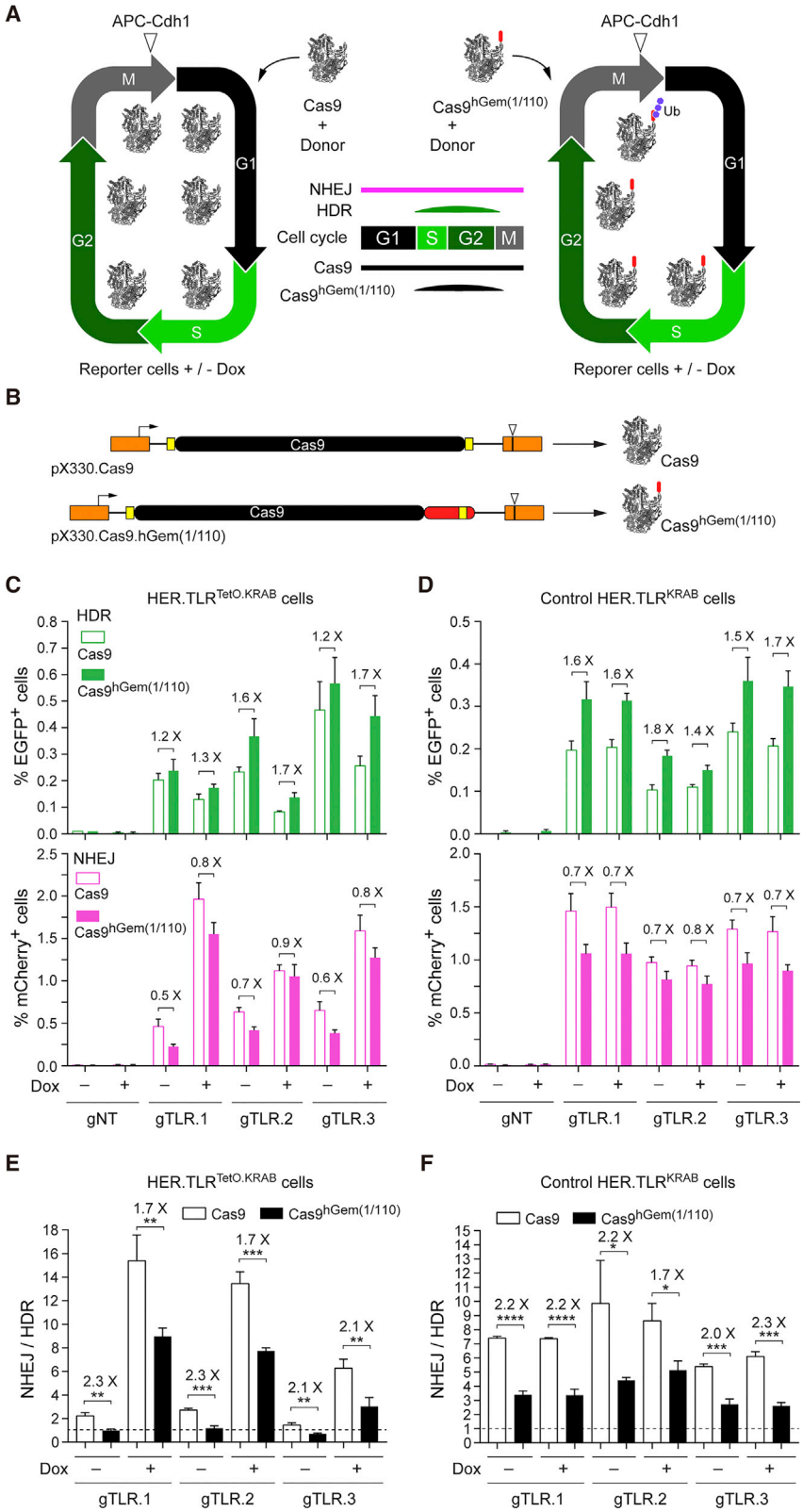

Figure 6. Investigating Gene-Editing Outcomes at Euchromatin versus Heterochromatin Using Cell Cycle-Regulated Cas9

(A) Constitutive and cell cycle-dependent post-translational regulation of Cas9 activity. Regular Cas9 is stable throughout the cell cycle, inducing DSBs at stages in which HDR is either not active or has to compete with NHEJ; Cas9$^{hGem(1/110)}$, in contrast, owing to APC/C-Cdh1-mediated ubiquitination (Ub) and subsequent proteolysis at the M-to-G1 transition, preferentially accumulates during the HDR-permissive S-G2 phases. (B) Schematics of the main components of Cas9 and Cas9$^{hGem(1/110)}$ expression constructs. Orange box with broken arrow, chimeric regulatory elements including the human cytomegalovirus *immediate-early* enhancer and the chicken *β-actin* promoter; orange box with vertical arrowhead, bovine *growth hormone* polyadenylation signal; yellow boxes, nuclear localization signals; black oval, *Cas9* ORF; red oval, DNA coding for the first 110 residues of human Geminin, hGem(1/110). (C) Dual-color flow cytometric quantification of HDR and NHEJ events at euchromatin versus heterochromatin using Cas9 or Cas9$^{hGem(1/110)}$. HER.TLR$^{TetO.KRAB}$ cells, incubated or not incubated with Dox, were exposed to Plasmid^{d} and the indicated gRNAs together with Cas9 (open bars) or Cas9$^{hGem(1/110)}$ (solid bars). (D) Dual-color flow cytometric quantification of HDR and NHEJ events induced by Cas9 or Cas9$^{hGem(1/110)}$ in control HER.TLR^{KRAB} cells. HER.TLR^{KRAB} cells, treated or not treated with Dox, were exposed to Plasmid^{d} and the indicated gRNAs together with Cas9 (open bars) or Cas9$^{hGem(1/110)}$ (solid bars). (E) Relative participation of HDR and NHEJ pathways during plasmid-mediated repair of DSBs created at heterochromatin versus euchromatin. Net result of the data shown in (C) corresponds to the ratios between the frequencies of NHEJ and HDR in HER.TLR$^{TetO.KRAB}$ cells exposed or not exposed to Dox. Bars represent mean ± SD of three independent experiments (biological replicates done on different days). The p values varied from a minimum of 5×10^{-4} to a maximum of 8.5×10^{-3}; $p < 0.05$ was considered significant. (F) Relative participation of HDR and NHEJ pathways during plasmid-mediated repair of DSBs in control HER.TLR^{KRAB} cells. Net result of the data shown in (D) corresponds to the ratios between the frequencies of NHEJ and HDR in HER.TLR^{KRAB} cells incubated or not incubated with Dox. Bars represent mean ± SD of three independent experiments (biological replicates done on different days). The p values varied from a minimum of $<1 \times 10^{-4}$ to a maximum of 3.7×10^{-2}; $p < 0.05$ was considered significant.

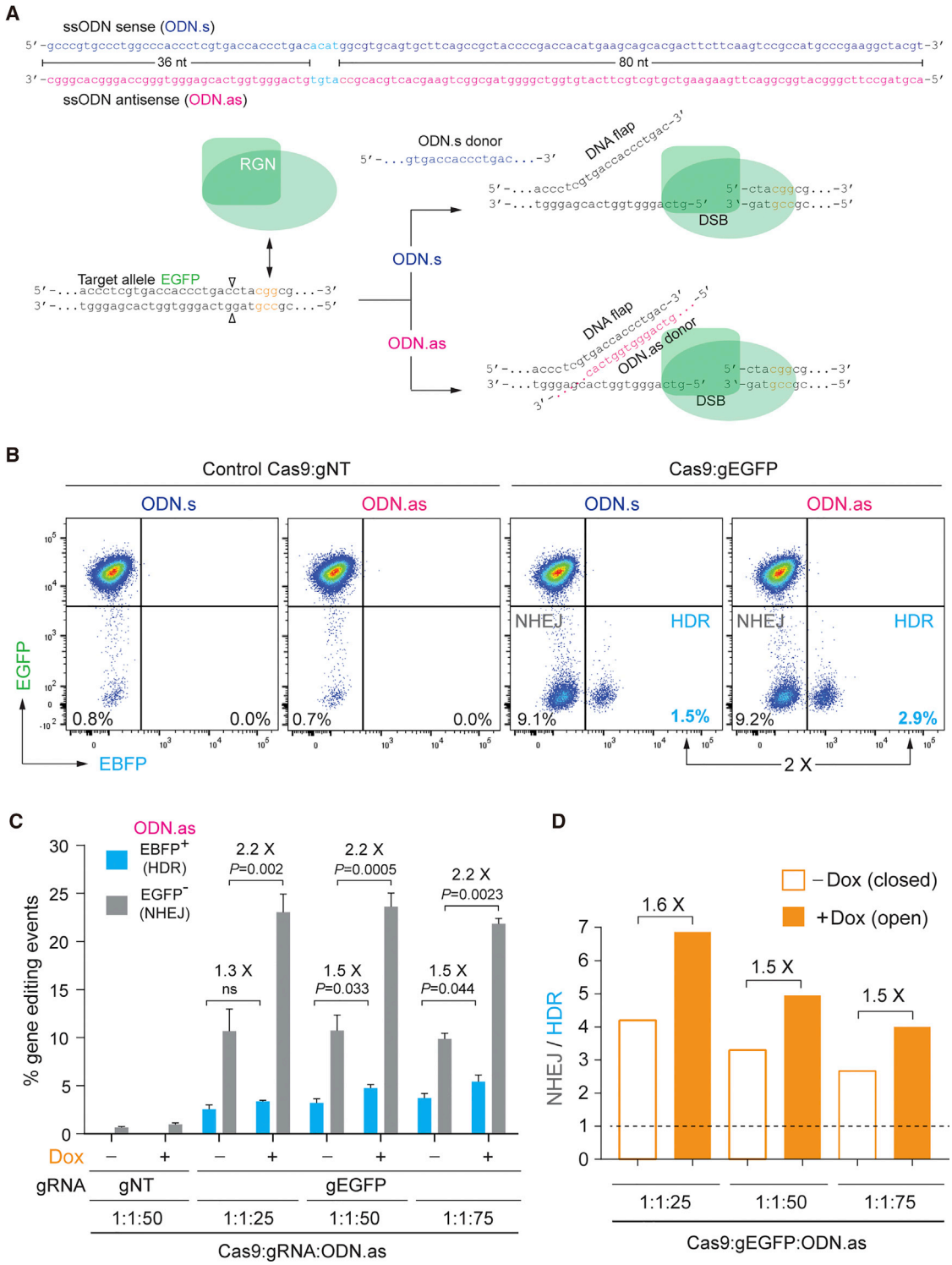

Figure 7. Gene-Editing Endpoints at Euchromatin versus Heterochromatin after ODN Donor Delivery in HEK.EGFP$^{TetO.KRAB}$ Cells

(A) Schematics of ODN design and target site before and after RGN engagement. The RGN complex Cas9:gEGFP is presumed to generate a 3′-ended DNA flap complementary and non-complementary to ODN.as and ODN.s, respectively. HDR-based gene editing with ODN.s and ODN.as donors should result in *EGFP*-to-*EBFP* conversion via the knocking in of exogenous DNA encoding the EBFP flurochrome (cyan nucleotides) flanked by sequences complementary to the target site, i.e., 36- and

(legend continued on next page)

Interestingly, in contrast to the previous experiments in which HDR frequencies at euchromatin and heterochromatin were similar or higher at the latter state (Figures 2, 3, 5, and 6D), these final experiments deploying ODNs showed a somewhat higher frequency of HDR at euchromatin (Figure 7C). Possibly this is explained by the fact that short single-stranded ODNs engage genomic DSBs differently from long double-stranded donors. Indeed, working models for ODN-based HDR include the bridge and template models, in which only the latter shares steps with canonical HDR.[30] Yet, the measurable increase in ODN-based HDR at euchromatin (up to 1.5-fold) was lower than that observed for NHEJ (2.2-fold), thus still yielding higher NHEJ to HDR ratios at euchromatin (Figure 7D), as observed in gene-editing experiments using the other types of donor DNA, i.e., IDLV and plasmid templates (Figures 2, 3, and 5).

In conclusion, we report that, in contrast to the higher NHEJ frequencies at euchromatin over heterochromatin, HDR-mediated gene editing efficiencies are generally less impacted by the chromatin structure. Hence, albeit varying in degree, there is a KAP1-HP1-dependent shift in the relationship between exogenous DNA-derived HDR and mutagenic NHEJ events at single DSBs in human cells. This shift toward HDR takes place regardless of whether the donor DNA is presented in target cell nuclei as IDLVs, recombinant plasmids, or single-stranded ODNs, which together make up the most common sources of exogenous genetic information used in programmable nuclease-assisted genome-editing procedures.

DISCUSSION

HDR-based genome editing is key for numerous research applications, including modeling, screening, or correcting genotypes underlying human disorders in stem and/or progenitor cells. Unfortunately, in most instances accurate HDR takes place much less frequently than mutagenic NHEJ.[3,4] Thus, identifying the biological parameters governing this strong DNA repair bias has both scientific and practical relevance. In this study, we have investigated the outcome of the interaction between the molecular tools necessary for HDR-based gene editing and the chromatin structure of target sequences. In particular, we assessed RGN-induced gene editing endpoints established after the engagement of donors of viral, non-viral, and synthetic origins, with isogenic target sequences located either in euchromatin or heterochromatin controlled by the absence or presence, respectively, of the KAP1-HP1-dependent remodeling apparatus. We found that the relative proportions of gene-editing endpoints resulting from mutagenic NHEJ and precise HDR events can depend to a significant degree on the chromatin conformation of target sequences, with a shift occurring toward HDR events at heterochromatin assembled via the KRAB-mediated recruitment of gene-silencing complexes (Figure 8). This bias can vary in its extent, such as when using IDLVs versus plasmids as sources of exogenous DSB-repairing substrates.

Our findings indicate that the relative frequencies of gene-editing endpoints (i.e., wanted HDR vis-à-vis unwanted NHEJ events) can be influenced not only by selecting different types of donor DNA structures but also, critically, by the epigenomic landscape of specific cell types or the dynamic and epigenetically regulated chromatin changes underlying organismal development and cellular differentiation. Hence, the chromatin context of target sequences in specific cell types or cell differentiation stages should be taken into account whenever applying HDR-based gene editing procedures. For instance, the probability for isolating gene-edited cell clones devoid of NHEJ-derived allelic mutations might be higher if target sequences are embedded in HDR-susceptible and NHEJ-refractory heterochromatin as opposed to NHEJ-prone euchromatin. In this regard, increasing programmable nuclease accessibility by applying chromatin-remodeling agents, e.g., programmable trans-activators, histone deacetylase inhibitors, and/or DNA methyltransferase inhibitors, might in fact be counterproductive. Indeed, in contrast to desirable HDR events, mutagenic NHEJ footprints can increase significantly due to enhanced physical and temporal exposure of target alleles to programmable nucleases, especially during the aforementioned cell cycle stages in which HDR is not operative. Conversely, and prior to our work somewhat counterintuitively, HDR-based gene editing procedures might profit from transiently addressing programmable DNA-binding complexes with epigenetic repressors (e.g., KRAB) to the vicinity of euchromatic target genes. Such approaches will, however, require the timely delivery of additional molecular tools, e.g., catalytically dead Cas9 orthologs fused to KRAB, so that target sequences become epigenetically remodeled before they are exposed to DNA-editing agents. Instead, we have explored a simpler strategy in which a single modified Cas9 nuclease, i.e., Cas9-hGem(1/110),[22] is used to guarantee that DSB formation is largely restricted to the HDR-permissive S-G2 phases of the cell cycle. Importantly, we demonstrate that, regardless of the KAP1-HP1-regulated compaction statuses of target DNA, downregulating Cas9 activity during G1 leads to a significant reduction in the ratios between NHEJ and HDR (Figures 6E and 6F).

Currently, there is a paucity of knowledge about the mechanisms responsible for the repairing of DSBs located within different chromatin contexts in mammalian cells. In recent years, however, the classical view that heterochromatin simply poses a barrier to

80-nt-long arms. Open arrowheads, position of the DSB induced by Cas9:gEGFP; orange triplet, PAM. (B) Probing HDR-based gene editing with sense and antisense ODNs. HEK.EGFP$^{Tet.KRAB}$ cells were transfected with ODN.s or with ODN.as, each mixed with expression plasmids coding for either non-cutting Cas9:gNT or cutting Cas9:gEGFP complexes. HDR and NHEJ quantification in HEK.EGFP$^{Tet.KRAB}$ cells was assessed by EBFP- and EGFP-directed flow cytometry, respectively. (C) ODN-based gene editing. Dual-color flow cytometric quantification of HDR and NHEJ frequencies in HEK.EGFP$^{TetO.KRAB}$ cells is shown. HER.TLR$^{TetO.KRAB}$ cells, incubated (+) or not incubated (–) with Dox, were exposed to the indicated experimental conditions. Bars correspond to mean ± SD of the indicated number (n) of independent experiments (biological replicates done on different days). (D) Relative participation of HDR and NHEJ pathways during ODN-mediated repair of DSBs taking place at heterochromatin versus euchromatin. Panel D displays the results shown in (C) as the ratios between the frequencies of NHEJ and HDR in HEK.EGFP$^{TetO.KRAB}$ cells exposed or not exposed to Dox.

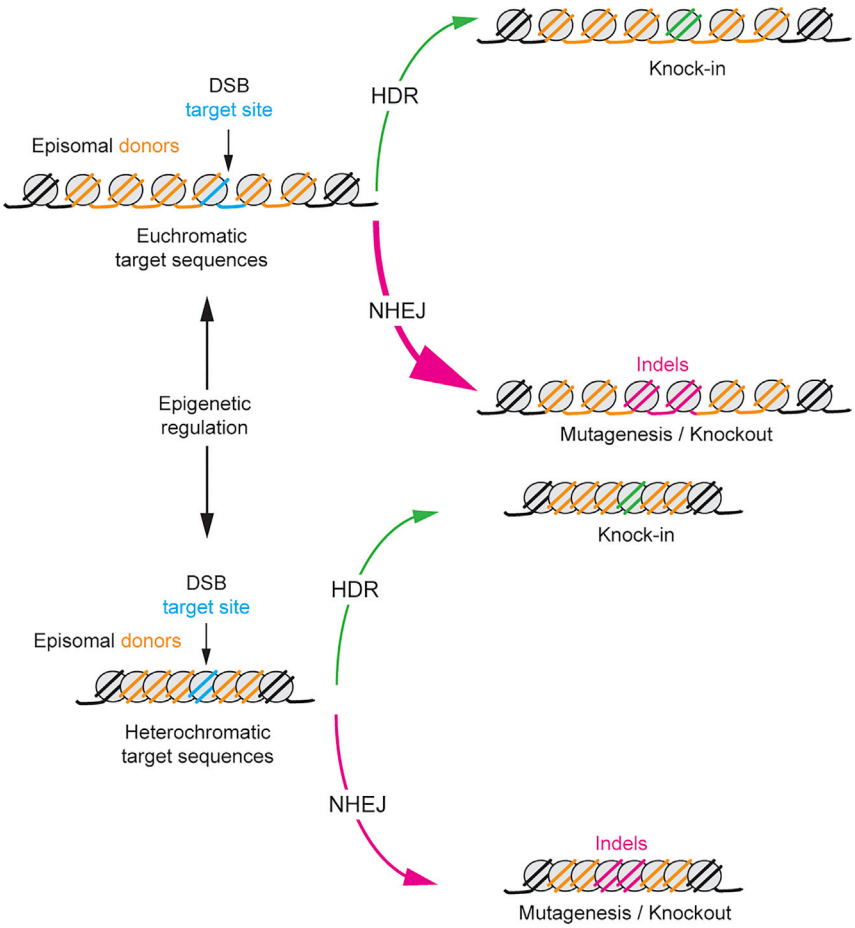

Figure 8. Summarizing Illustration on the Role of Alternative Chromatin Structures on Gene-Editing Outcomes

The thickness of the curved arrows represents the relative contribution of homology-directed repair (HDR) and non-homologous end joining (NHEJ) pathways to gene-editing endpoints at euchromatin versus KRAB-controlled heterochromatin.

the DNA damage response (DDR) is changing into one in which heterochromatin and heterochromatin-associated proteins are active participants in it.[31] For instance, SENP7 interacts with KAP1 via HP1α, resulting in the deSUMOylation of KAP1.[32] The removal of this post-translational modification from KAP1 promotes the transient release of the co-repressors CHD3 and SETDB1 from chromatin, which, in turn, creates a cellular milieu favorable for HDR-mediated DSB repair.[32] A similar milieu is conferred by the MRE11-RAD50-NBS1 complex-dependent recruitment of the histone acetyltransferase Trrap-Tip60 to heterochromatic DSBs.[33] Interestingly, in HP1α-knockdown cells, in contrast to the buildup of the NHEJ factor XRCC4 at laser-induced DNA lesions, there is a marked reduction of the HDR factors RAD51 and BRCA1 at these lesions.[34] Subsequent experiments, based on exposing cells to the restriction enzyme AsiSI, provided additional support for the participation of heterochromatin-resident HP1 proteins in associating BRCA1 with DSBs and facilitating HDR.[35]

Collectively, these data provide compelling evidence for an active role of HDR during heterochromatic DSB repair, involving an intricate interplay among histone marks (e.g., H3K9me3), chromatin-remodeling factors (e.g., HP1 isoforms, CHD3, Trrap-Tip60, and KAP1), and DNA repair proteins (e.g., BRCA1, RPA, and RAD51). It is worth mentioning, however, that, for the most part, these experiments have relied on generating supra-physiological amounts of different types of DSBs throughout the genome by ionizing radiation, laser microirradiation, or restriction enzyme exposure. Moreover, the relative proportions between HDR and NHEJ events at isogenic sequences with distinct chromatin states in cells exposed to different donor DNA substrates was not investigated. Finally, although certain DDR processes seem to have a bias for repairing heterochromatic DSBs, e.g., ATM-mediated phosphorylation of KAP1,[36] some others appear to lack this bias, e.g., p150CAF-1-mediated recruitment of HP1α to DSBs.[34] It should thus be very instructive investigating which DDR components and mechanisms are more specific to heterochromatin over euchromatin or are instead shared by both compartments.

Concluding, in this study, we implemented cellular assays based on epigenetically regulated genetic reporters, donor DNA templates, and RGNs for the simultaneous quantification of HDR- and NHEJ-derived gene editing events at single-target sequences subjected to distinct chromatin conformations. The resulting data expand the aforementioned findings by providing direct experimental evidence for a role of the chromatin structure on the differential engagement of the two major DNA repair pathways in mammalian cells. The recruitment of DDR factors and DNA recombination substrates into a well-defined genetic and epigenetic environment offered by these live-cell tracking systems should aid detailed investigations into the mechanisms of DDR under different chromatin contexts, as well as their interplay with other cellular mechanisms and DNA metabolic processes such as replication. Finally, as illustrated herein through experiments testing HDR substrates of viral, non-viral, and synthetic origins and cell cycle-timed Cas9 proteins, this epigenetically regulated experimental system might also serve for assessing *in cellula* the impact of chromatin on novel gene-editing protocols involving, among others, donor DNA substrates with different structures and compositions, newly engineered Cas9 proteins, NHEJ-inhibiting reagents,[37,38] and as of yet unexploited programmable nuclease systems.[39,40]

MATERIALS AND METHODS

Cells

The human embryonic retinoblasts HER.TLR$^{TetO.KRAB}$ and their control *TetO*-negative counterparts HER.TLR^{KRAB} were generated and cultured as detailed elsewhere[10] (and likewise for the human embryonic kidney cells HEK.EGFP$^{TetO.KRAB}$).[10] The HEK293T cells (American Type Culture Collection) used for the generation of IDLV^{d} preparations were maintained in DMEM (Thermo Fisher Scientific) supplemented with 10% fetal bovine serum (FBS; Thermo Fisher Scientific). The HEK.EGFP$^{TetO.KRAB}$ line is a single-cell-derived clone; the HER.TLR$^{TetO.KRAB}$ cells are polyclonal.[10] The cells used in this study were mycoplasma free and were kept at 37°C in a humidified-air 10% CO_2 atmosphere.

Recombinant DNA

The gRNA acceptor construct S7_pUC.U6.sgRNA.BveI-stuffer contains a human *U6* RNA polymerase III (Pol III) promoter and terminator sequence for gRNA expression.[10] The gRNA expression plasmids Z42_pgTLR.1, Z44_pgTLR.2, AW26_pgTLR.3, AM51_pgNT, and AX03_pgEGFP were generated by ligating the annealed oligonucleotide pairs listed in Table S1 into BveI-digested S7_pUC.U6.sgRNA.BveI-stuffer. The plasmid hCas9 was used for expressing the *S. pyogenes* Cas9 nuclease (Addgene plasmid 41815).[41] The sequence and annotated map of construct AX63_pTHG.donor, used for HDR-mediated editing of *EGFP* into *EBFP*, are shown in the Supplemental Materials and Methods. The Addgene plasmid 31475 pCVL SFFV d14 GFP,[23] herein named Plasmid^{d}, served as a source of donor DNA in the gene-editing experiments performed on HER.TLR$^{TetO.KRAB}$ and HER.TLR^{KRAB} cells. Plasmid^{d} is a lentiviral vector construct that harbors the *TLR*-targeting donor template EGFPtrunc.[23] The pair of isogenic expression plasmids pX330-U6-Chimeric_BB-CBh-hSpCas9[42] and pX330-U6-Chimeric_BB-CBh-hSpCas9-hGem (1/110)[22] were obtained from Addgene (plasmids 42230 and 71707, respectively). The former and latter constructs are herein dubbed pX330.Cas9 and pX330.Cas9.hGem(1/110), respectively.

DNA Transfections

HER.TLR$^{TetO.KRAB}$ cells were kept for 10 days in medium lacking or containing Dox at a final concentration of 0.5 μg mL^{-1}. Next, each of these cell cultures (i.e., with and without Dox) were seeded 1 day before DNA transfections in wells of 24-well plates (Greiner Bio-One) (Tables S2–S7; Figure S4A). The DNA transfections were initiated by adding 1 mg mL^{-1} linear 25 kDa polyethyleneimine (PEI; Polysciences) to the different plasmid mixtures diluted in 50 μL 150 mM NaCl (Tables S2–S7; Figure S4A). After vortexing for 10 s, the DNA-PEI complexes were let to be formed for 15 min at room temperature, after which they were directly added to the medium of the cell cultures. The different transfection mixtures were substituted 6–8 h later by regular culture medium with or without Dox. At 3 days post-transfection, the cells were sub-cultured every 3–4 days for a period of 11 days, and the frequencies of EGFP- and mCherry-positive cells in the cultures were determined by flow cytometry (Figure S4A). To activate transgene expression, the cultures initially lacking Dox were exposed to Dox (0.5 μg mL^{-1}) for 10 days, after which the frequencies of EGFP- and mCherry-positive cells were also determined in these cultures by flow cytometry (Figure S4A). The transfection protocols and experimental design applied to the control *TetO*-negative HER.TLR^{KRAB} cells were similar to those applied to the *TetO*-positive HER.TLR$^{TetO.KRAB}$ cells (Table S5; Figure S4B).

HEK.EGFP$^{TetO.KRAB}$ cells were cultured for 7 days in the presence or absence of Dox at a final concentration of 0.2 μg mL^{-1}. Next, the cells were seeded 1 day before DNA transfections in wells of 24-well plates (Greiner Bio-One) (Tables S8–S10; Figure S4C). The DNA transfections started by adding 1 mg mL^{-1} PEI to the different plasmid mixtures diluted in 50 μL 150 mM NaCl (Tables S8–S10; Figure S4C). After vortexing for 10 s, the DNA-PEI complexes were let to be formed for 15 min at room temperature, after which they were directly added to the medium of the cell cultures. The various transfection mixtures were replaced 6–8 h later by regular culture medium with or without Dox. At 3 days post-transfection, the cells were sub-cultured every circa 3 days for a period of 7 days, and the frequencies of EBFP-positive and EGFP-negative cells in the cultures containing Dox were determined by flow cytometry (Figure S4C). To activate transgene expression, the cultures that initially had not received Dox were incubated in the presence of Dox (0.2 μg mL^{-1}) for an additional 7-day period, after which the frequencies of EBFP-positive and EGFP-negative cells were also determined in these cultures by flow cytometry (Figure S4C).

IDLV Production and Titration

The assembly of IDLV^{d} particles was carried out by transient transfections of HEK293T cells with lentiviral vector construct Plasmid^{d},[23] together with packaging plasmid AM16_psPAX2.IN^{D116N}[43] and vesicular stomatitis virus glycoprotein-G-pseudotyping construct pLP/VSVG (Thermo Fisher Scientific), as detailed previously.[43,44] The protocols for the concentration and purification of IDLV^{d} particles released into the producer-cell culture medium were equally detailed elsewhere.[43,44] Finally, the physical particle titers of the resulting IDLV^{d} stocks were determined by measuring the HIV-1 p24^{gag} antigen with the aid of the RETRO-TEK HIV-1 p24 ELISA kit, following the manufacturer's instructions (Gentaur Molecular Products).

Gene-Editing Experiments with Single-Stranded ODNs

The 120-nt-long, single-stranded ODNs ODN.s (5′-GCCCGTGCCCTGGCCCACCCTCGTGACCACCCTGACACATGGCGTGCAGTGCTTCAGCCGCTACCCCGACCACATGAAGCAGCACGACTTCTTCAAGTCCGCCATGCCCGAAGGCTACGT-3′) and ODN.as (5′-ACGTAGCCTTCGGGCATGGCGGACTTGAAGAAGTCGTGCTGCTTCATGTGGTCGGGGTAGCGGCTGAAGCACTGCACGCCATGTGTCAGGGTGGTCACGAGGGTGGGCCAGGGCACGGGC-3′) were custom synthesized and high-performance liquid chromatography purified (Eurofins Scientific). These ODNs were reconstituted in a solution of 10 mM Tris-Cl and 1 mM EDTA (pH 8.0) to a concentration of 100 pmol μL^{-1}. A 50-fold dilution of this stock was divided in aliquots and stored at −20°C prior to transfection. The

ODNs were transfected together with RGN-encoding plasmids into HEK.EGFP$^{TetO.KRAB}$ cells cultured in the absence or presence of Dox (0.2 μg mL^{-1}), using the previously described PEI-based protocol and the DNA mixtures detailed in Tables S9 and S10.

Flow Cytometry

The measurements of EGFP-positive, EGFP-negative, EBFP-positive, and mCherry-positive cells were performed using a BD LSR II flow cytometer (BD Biosciences). The data were analyzed with the support of FlowJo 10.1 software (Tree Star) or BD FACSDiva 6.1.3 software (BD Biosciences). Mock-transfected cells served for establishing background fluorescence thresholds. At least 40,000 viable single cells were analyzed per sample.

Statistical Analysis

The comparison of the indicated datasets resulting from independent experiments (biological replicates done on different days) was analyzed by applying two-tailed Student's t tests ($p < 0.05$ considered significant). The GraphPad Prism 6 software package was used for this analysis.

SUPPLEMENTAL INFORMATION

Supplemental Information can be found with this article online at https://doi.org/10.1016/j.omtn.2019.02.009.

AUTHOR CONTRIBUTIONS

J.M.J. and X.C. generated reagents and performed the experiments together with J.L. M.A.F.V.G., J.M.J., and X.C. designed the experiments and analyzed the data. M.A.F.V.G. conceived and initiated the research. M.A.F.V.G. wrote the manuscript with the help of the other authors.

CONFLICTS OF INTEREST

The authors have none to declare.

ACKNOWLEDGMENTS

The authors thank Martijn Rabelink (Department of Cell and Chemical Biology, LUMC, Leiden, the Netherlands) for carrying out the p24^{gag} ELISA measurements. The authors also thank Rob Hoeben (Department of Cell and Chemical Biology, LUMC, Leiden, the Netherlands) and Ignazio Maggio (Department of Paediatrics, LUMC, Leiden, the Netherlands) for their critical reading of the manuscript. The research in our laboratory is supported by the Dutch Prinses Beatrix Spierfonds (W.OR11-18), the European Union's Horizon 2020 research and innovation programme under the Marie Skłodowska-Curie grant agreement 765269 (IMGENE – Improving genome editing efficiency), the Duchenne Parent Project NL (17.012), and ProQR Therapeutics. X.C. held a Ph.D. research fellowship from the China Scholarship Council-Leiden University Joint Scholarship Programme.

REFERENCES

1. Kim, H., and Kim, J.S. (2014). A guide to genome engineering with programmable nucleases. Nat. Rev. Genet. *15*, 321–334.
2. Maggio, I., and Gonçalves, M.A. (2015). Genome editing at the crossroads of delivery, specificity, and fidelity. Trends Biotechnol. *33*, 280–291.
3. Chang, H.H.Y., Pannunzio, N.R., Adachi, N., and Lieber, M.R. (2017). Non-homologous DNA end joining and alternative pathways to double-strand break repair. Nat. Rev. Mol. Cell Biol. *18*, 495–506.
4. Heyer, W.D. (2015). Regulation of recombination and genomic maintenance. Cold Spring Harb. Perspect. Biol. *7*, a016501.
5. Kouzarides, T. (2007). Chromatin modifications and their function. Cell *128*, 693–705.
6. Chen, X., and Gonçalves, M.A.F.V. (2018). DNA, RNA, and protein tools for editing the genetic information in human cells. iScience *6*, P247–P263.
7. Bultmann, S., Morbitzer, R., Schmidt, C.S., Thanisch, K., Spada, F., Elsaesser, J., Lahaye, T., and Leonhardt, H. (2012). Targeted transcriptional activation of silent oct4 pluripotency gene by combining designer TALEs and inhibition of epigenetic modifiers. Nucleic Acids Res. *40*, 5368–5377.
8. Daboussi, F., Zaslavskiy, M., Poirot, L., Loperfido, M., Gouble, A., Guyot, V., Leduc, S., Galetto, R., Grizot, S., Oficjalska, D., et al. (2012). Chromosomal context and epigenetic mechanisms control the efficacy of genome editing by rare-cutting designer endonucleases. Nucleic Acids Res. *40*, 6367–6379.
9. Valton, J., Dupuy, A., Daboussi, F., Thomas, S., Maréchal, A., Macmaster, R., Melliand, K., Juillerat, A., and Duchateau, P. (2012). Overcoming transcription activator-like effector (TALE) DNA binding domain sensitivity to cytosine methylation. J. Biol. Chem. *287*, 38427–38432.
10. Chen, X., Rinsma, M., Janssen, J.M., Liu, J., Maggio, I., and Gonçalves, M.A. (2016). Probing the impact of chromatin conformation on genome editing tools. Nucleic Acids Res. *44*, 6482–6492.
11. Chen, X., Liu, J., Janssen, J.M., and Gonçalves, M.A.F.V. (2017). The chromatin structure differentially impacts high-specificity CRISPR-Cas9 nuclease strategies. Mol. Ther. Nucleic Acids *8*, 558–563.
12. Daer, R.M., Cutts, J.P., Brafman, D.A., and Haynes, K.A. (2017). The impact of chromatin dynamics on Cas9-mediated genome editing in human cells. ACS Synth. Biol. *6*, 428–438.
13. Jensen, K.T., Fløe, L., Petersen, T.S., Huang, J., Xu, F., Bolund, L., Luo, Y., and Lin, L. (2017). Chromatin accessibility and guide sequence secondary structure affect CRISPR-Cas9 gene editing efficiency. FEBS Lett. *591*, 1892–1901.
14. Verkuijl, S.A., and Rots, M.G. (2019). The influence of eukaryotic chromatin state on CRISPR-Cas9 editing efficiencies. Curr. Opin. Biotechnol. *55*, 68–73.
15. Urrutia, R. (2003). KRAB-containing zinc-finger repressor proteins. Genome Biol. *4*, 231.
16. Ecco, G., Imbeault, M., and Trono, D. (2017). KRAB zinc finger proteins. Development *144*, 2719–2729.
17. Groner, A.C., Meylan, S., Ciuffi, A., Zangger, N., Ambrosini, G., Dénervaud, N., Bucher, P., and Trono, D. (2010). KRAB-zinc finger proteins and KAP1 can mediate long-range transcriptional repression through heterochromatin spreading. PLoS Genet. *6*, e1000869.
18. Iyengar, S., and Farnham, P.J. (2011). KAP1 protein: an enigmatic master regulator of the genome. J. Biol. Chem. *286*, 26267–26276.
19. Doudna, J.A., and Charpentier, E. (2014). Genome editing. The new frontier of genome engineering with CRISPR-Cas9. Science *346*, 1258096.
20. Wanisch, K., and Yáñez-Muñoz, R.J. (2009). Integration-deficient lentiviral vectors: a slow coming of age. Mol. Ther. *17*, 1316–1332.
21. Anders, C., Niewoehner, O., Duerst, A., and Jinek, M. (2014). Structural basis of PAM-dependent target DNA recognition by the Cas9 endonuclease. Nature *513*, 569–573.
22. Gutschner, T., Haemmerle, M., Genovese, G., Draetta, G.F., and Chin, L. (2016). Post-translational regulation of Cas9 during G1 enhances homology-directed repair. Cell Rep. *14*, 1555–1566.
23. Certo, M.T., Ryu, B.Y., Annis, J.E., Garibov, M., Jarjour, J., Rawlings, D.J., and Scharenberg, A.M. (2011). Tracking genome engineering outcome at individual DNA breakpoints. Nat. Methods *8*, 671–676.

24. Kuscu, C., Arslan, S., Singh, R., Thorpe, J., and Adli, M. (2014). Genome-wide analysis reveals characteristics of off-target sites bound by the Cas9 endonuclease. Nat. Biotechnol. *32*, 677–683.

25. Wu, X., Scott, D.A., Kriz, A.J., Chiu, A.C., Hsu, P.D., Dadon, D.B., Cheng, A.W., Trevino, A.E., Konermann, S., Chen, S., et al. (2014). Genome-wide binding of the CRISPR endonuclease Cas9 in mammalian cells. Nat. Biotechnol. *32*, 670–676.

26. O'Geen, H., Henry, I.M., Bhakta, M.S., Meckler, J.F., and Segal, D.J. (2015). A genome-wide analysis of Cas9 binding specificity using ChIP-seq and targeted sequence capture. Nucleic Acids Res. *43*, 3389–3404.

27. Bou Kheir, T., and Lund, A.H. (2010). Epigenetic dynamics across the cell cycle. Essays Biochem. *48*, 107–120.

28. Sakaue-Sawano, A., Kurokawa, H., Morimura, T., Hanyu, A., Hama, H., Osawa, H., Kashiwagi, S., Fukami, K., Miyata, T., Miyoshi, H., et al. (2008). Visualizing spatiotemporal dynamics of multicellular cell-cycle progression. Cell *132*, 487–498.

29. Richardson, C.D., Ray, G.J., DeWitt, M.A., Curie, G.L., and Corn, J.E. (2016). Enhancing homology-directed genome editing by catalytically active and inactive CRISPR-Cas9 using asymmetric donor DNA. Nat. Biotechnol. *34*, 339–344.

30. Storici, F., Snipe, J.R., Chan, G.K., Gordenin, D.A., and Resnick, M.A. (2006). Conservative repair of a chromosomal double-strand break by single-strand DNA through two steps of annealing. Mol. Cell. Biol. *26*, 7645–7657.

31. Watts, F.Z. (2016). Repair of DNA Double-Strand Breaks in Heterochromatin. Biomolecules *6*, 47.

32. Garvin, A.J., Densham, R.M., Blair-Reid, S.A., Pratt, K.M., Stone, H.R., Weekes, D., Lawrence, K.J., and Morris, J.R. (2013). The deSUMOylase SENP7 promotes chromatin relaxation for homologous recombination DNA repair. EMBO Rep. *14*, 975–983.

33. Murr, R., Loizou, J.I., Yang, Y.G., Cuenin, C., Li, H., Wang, Z.Q., and Herceg, Z. (2006). Histone acetylation by Trrap-Tip60 modulates loading of repair proteins and repair of DNA double-strand breaks. Nat. Cell Biol. *8*, 91–99.

34. Baldeyron, C., Soria, G., Roche, D., Cook, A.J., and Almouzni, G. (2011). HP1alpha recruitment to DNA damage by p150CAF-1 promotes homologous recombination repair. J. Cell Biol. *193*, 81–95.

35. Lee, Y.H., Kuo, C.Y., Stark, J.M., Shih, H.M., and Ann, D.K. (2013). HP1 promotes tumor suppressor BRCA1 functions during the DNA damage response. Nucleic Acids Res. *41*, 5784–5798.

36. Goodarzi, A.A., Noon, A.T., Deckbar, D., Ziv, Y., Shiloh, Y., Löbrich, M., and Jeggo, P.A. (2008). ATM signaling facilitates repair of DNA double-strand breaks associated with heterochromatin. Mol. Cell *31*, 167–177.

37. Chu, V.T., Weber, T., Wefers, B., Wurst, W., Sander, S., Rajewsky, K., and Kühn, R. (2015). Increasing the efficiency of homology-directed repair for CRISPR-Cas9-induced precise gene editing in mammalian cells. Nat. Biotechnol. *33*, 543–548.

38. Robert, F., Barbeau, M., Éthier, S., Dostie, J., and Pelletier, J. (2015). Pharmacological inhibition of DNA-PK stimulates Cas9-mediated genome editing. Genome Med. *7*, 93.

39. Chylinski, K., Makarova, K.S., Charpentier, E., and Koonin, E.V. (2014). Classification and evolution of type II CRISPR-Cas systems. Nucleic Acids Res. *42*, 6091–6105.

40. Burstein, D., Harrington, L.B., Strutt, S.C., Probst, A.J., Anantharaman, K., Thomas, B.C., Doudna, J.A., and Banfield, J.F. (2017). New CRISPR-Cas systems from uncultivated microbes. Nature *542*, 237–241.

41. Mali, P., Yang, L., Esvelt, K.M., Aach, J., Guell, M., DiCarlo, J.E., Norville, J.E., and Church, G.M. (2013). RNA-guided human genome engineering via Cas9. Science *339*, 823–826.

42. Cong, L., Ran, F.A., Cox, D., Lin, S., Barretto, R., Habib, N., Hsu, P.D., Wu, X., Jiang, W., Marraffini, L.A., and Zhang, F. (2013). Multiplex genome engineering using CRISPR/Cas systems. Science *339*, 819–823.

43. Pelascini, L.P., Janssen, J.M., and Gonçalves, M.A. (2013). Histone deacetylase inhibition activates transgene expression from integration-defective lentiviral vectors in dividing and non-dividing cells. Hum. Gene Ther. *24*, 78–96.

44. Pelascini, L.P., and Gonçalves, M.A. (2014). Lentiviral vectors encoding zinc-finger nucleases specific for the model target locus HPRT1. Methods Mol. Biol. *1114*, 181–199.

OMTN, Volume *16*

Supplemental Information

The Chromatin Structure of CRISPR-Cas9 Target DNA Controls the Balance between Mutagenic and Homology-Directed Gene-Editing Events

Josephine M. Janssen, Xiaoyu Chen, Jin Liu, and Manuel A.F.V. Gonçalves

SUPPLEMENTAL INFORMATION

Figure S1. Target sites of RGN complexes in the *TLR* construct. The target sequences for the RGN complexes Cas9:gTLR.1, Cas9:gTLR.2 and Cas9:gTLR.3 are indicated by horizontal lines linked to open boxes delimiting the respective PAM sequences. The positions of the site-specific DSBs generated by each RGN are marked (vertical open arrowheads). STOP, nonsense codon located within the *TLR* ORF.

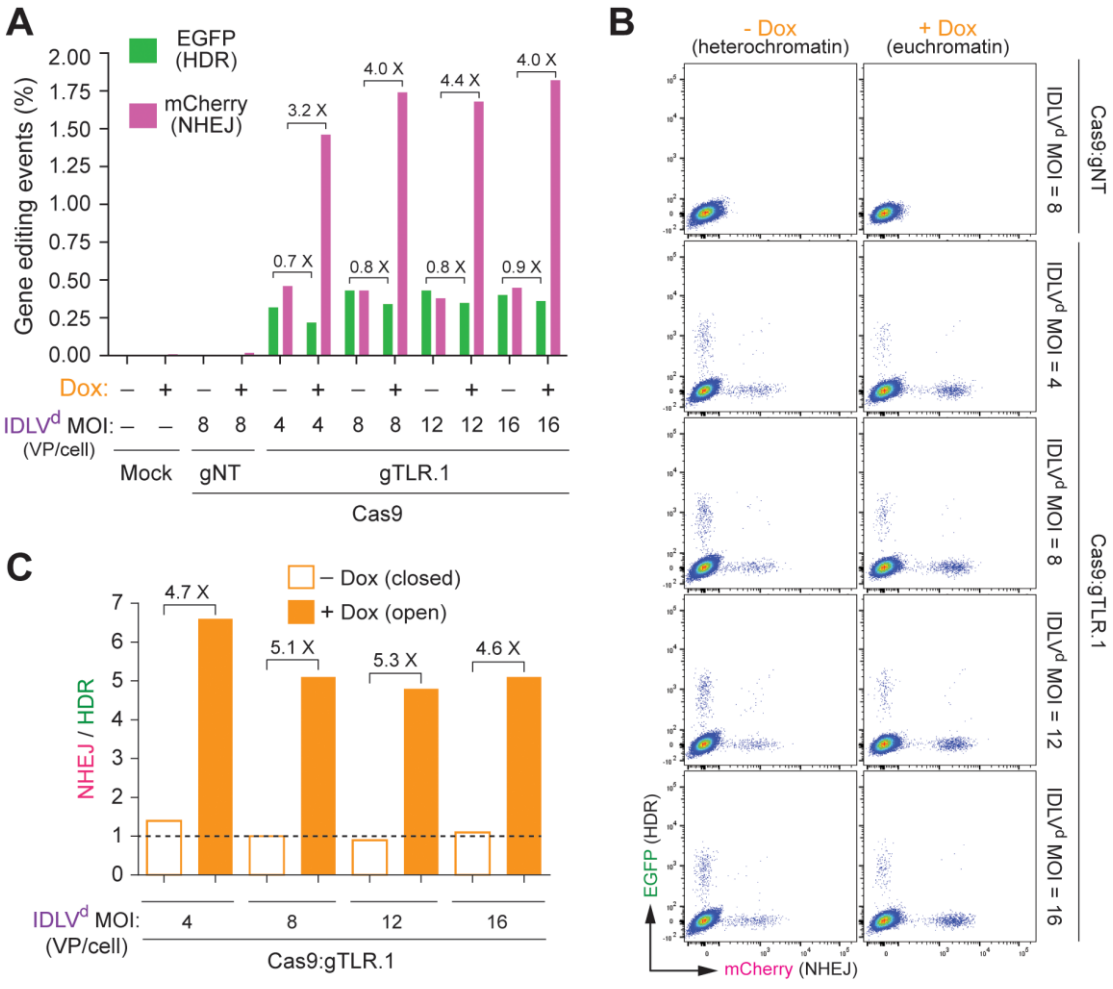

Figure S2. Gene editing endpoints at euchromatin versus heterochromatin after IDLV donor DNA delivery. (**A**) Dual-color flow cytometric quantification of HDR and NHEJ events in HER.TLR$^{TetO.KRAB}$ cells. HER.TLR$^{TetO.KRAB}$ cells were exposed to Cas9:gTLR.1 together with the indicated multiplicities of infection (MOI) of IDLV^{d}. Negative controls consisted of mock-treated cultures and of cultures exposed to a non-targeting gRNA (gNT), Cas9 and IDLV^{d} at an MOI of 8 vector particles per cell (VP/cell). The various experimental conditions were tested in HER.TLR$^{TetO.KRAB}$ reporter cells incubated in the absence (-) or in the presence (+) of doxycycline (Dox). The frequencies of HDR and NHEJ events in the various target cell populations were determined by measuring EGFP^{+} and mCherry^{+} cells, respectively. (**B**) Dot plots corresponding to HER.TLR$^{TetO.KRAB}$ cells transduced with different doses of IDLV^{d} particles and subjected to the indicated Dox regimens. (**C**) Relative participation of HDR and NHEJ pathways during IDLV-mediated repair of DSBs occurring at heterochromatin versus euchromatin. Data of panel **A** are presented as the ratios between the frequencies of NHEJ and HDR in HER.TLR$^{TetO.KRAB}$ cells not treated and treated with Dox.

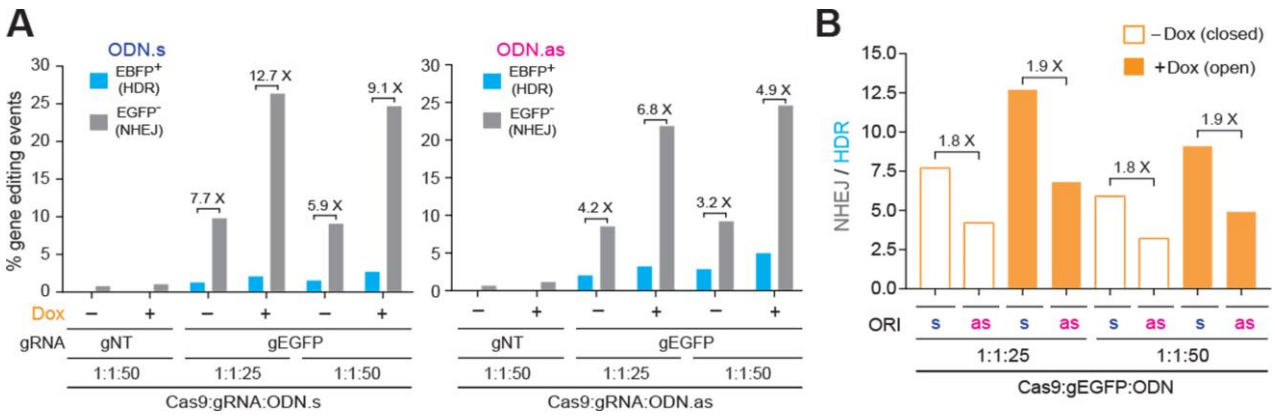

Figure S3. Gene editing endpoints at euchromatin versus heterochromatin in HEK.EGFP$^{TetO.KRAB}$ cells after transfection of ODNs with different polarities. (**A**) Testing the impact of chromatin structure on HDR-based gene editing with sense and antisense ODNs. HEK.EGFP^{TetKRAB} cells, incubated (+) or not incubated (-) with Dox, were exposed to the indicated experimental conditions. The frequencies of HDR and NHEJ were assessed by dual-color flow cytometry. (**B**) Relative participation of HDR and NHEJ pathways during the repair of euchromatic versus heterochromatic DSBs with ODNs with different polarities. Data of panel **A** displayed as the ratios between the

frequencies of NHEJ and HDR in HEK.EGFP$^{TetO.KRAB}$ cells treated and not treated with Dox.

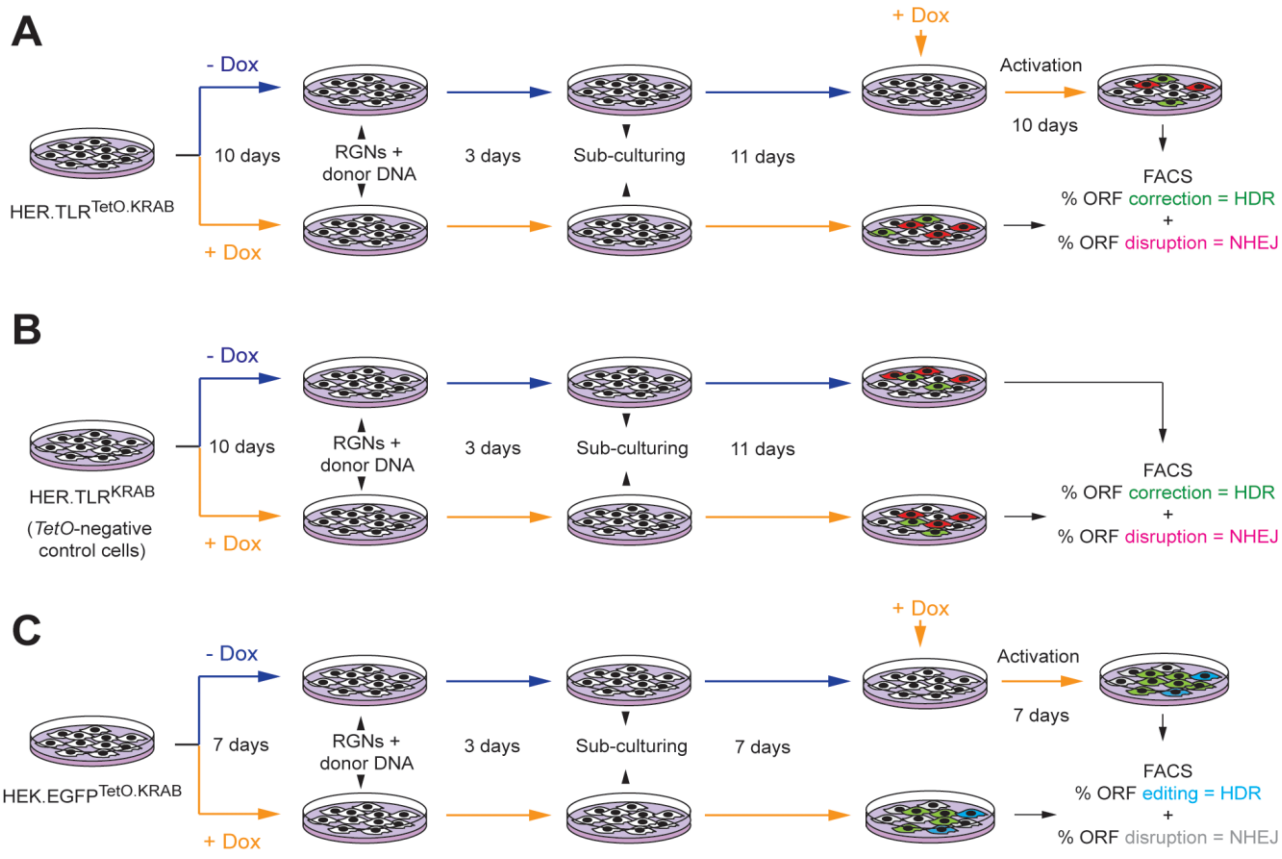

Figure S4. Schematic representation of the experimental settings used in the current study. The tTR-KRAB-expressing cells HER.TLR$^{TetO.KRAB}$ (**A**) contain the Dox-regulated *TLR*^{TetO} construct. The tTR-KRAB-expressing HER.TLR^{KRAB} reporter cells (**B**) have the Dox-insensitive *TLR* construct and were used as an isogenic control cellular system. The tTR-KRAB-expressing cells HEK.EGFP$^{TetO.KRAB}$ (**C**) contain the Dox-regulated *EGFP*^{TetO} construct. These reporter cells are transiently transfected in the presence or in the absence of Dox with different combinations of gene editing tools consisting of RGNs and donor DNA templates. After the generation of site-specific DSBs and the ensuing modification of target DNA sequences in cells subjected to both experimental settings (i.e. –Dox and +Dox), target gene expression is activated to quantifying by flow cytometry the frequencies of gene editing events resulting from the engagement of HDR and NHEJ pathways.

Table S1. Oligonucleotide pairs to generate the gRNA expression constructs expressing gTLR.1, gTLR.2, gTLR.3, gNT and gEGFP

Plasmids	Oligonucleotide pairs (5′- 3′)
Z42_pgTLR.1	5′-ACCGGTGAGCTCTTATTTGCGTA-3′ 5′-AAACTACGCAAATAAGAGCTCAC-3′
Z44_pTLR.2	5′-ACCGGGATAACAGGGTAATGTCG-3′ 5′-AAACCGACATTACCCTGTTATCC-3′
AW26_pTLR.3	5′-ACCGTAACAGGGTAATGTCGAGGC-3′ 5′-AAACGCCTCGACATTACCCTGTTA-3′
AM51_pgNT	5′-ACCGGTGAGCTCTTATTTGCGTAGCTAGCTGAC-3 5′-AAACGTCAGCTAGCTACGCAAATAAGAGCTCAC-3′
AX03_pgEGFP	5′-ACCGCTCGTGACCACCCTGACCTA-3′ 5′-AAACTAGGTCAGGGTGGTCACGAG-3′

Table S2. Experimental scheme corresponding to **Figure S2**

DONOR: IDLV^{d}	3.25 ×10^{5} HER.TLR$^{TetO.KRAB}$ cells per well of 24-well plates (500 µl medium per well with or without Dox)			
	PEI (1mg/ml)： 5.8 µl per well; <u>Ratio DNA / PEI equivalents = 6</u>			
Reagents	Cas9	gNT (Ctrl)	gTLR.1	Total (ng)
Construct length (bp)	9551	3056	3046	
DNA per well (ng)	**1327**	**423**		**1750**
	1327		**423**	**1750**
	1327			**1750**

Note 1: One day after transfecting plasmids expressing Cas9 and gTLR.1, IDLV^{d} particles were added at an MOI of 4, 8, 12 and 16 VP/cell; **Note 2**: One day after transfecting plasmids expressing Cas9 and gRNA^{NT}, IDLV^{d} particles were added at an MOIs of 8 VP/cell.

Table S3. Experimental scheme corresponding to **Figure 2** (**<u>Protocol A</u>**)

DONOR: IDLV^{d}	3.25 ×10^{5} HER.TLR$^{TetO.KRAB}$ cells per well of 24-well plates (500 µl medium per well with or without Dox)			
	PEI (1mg/ml)： 9.6 µl per well; <u>Ratio DNA / PEI equivalents = 10</u>			
Reagents	Cas9	gNT (Ctrl)	gTLR.1	Total (ng)
Construct length (bp)	9551	3056	3046	
DNA per well (ng)	**1327**	**423**		**1750**
	1327		**423**	**1750**
	1327			**1750**

Note: One day after transfection of the indicated plasmids, IDLVd particles were added at an MOI of 8 VP/cell.

Table S4. Experimental scheme corresponding to **Figure 2** (**Protocol B**)

DONOR: IDLV[d]	3.25 ×10[5] HER.TLR[TetO.KRAB] cells per well of 24-well plates (500 µl medium per well with or without Dox)				
	PEI (1mg/ml)： 5.8 µl per well; Ratio DNA / PEI equivalents = 6				
Reagents	Cas9	gNT (Ctrl)	gTLR.1	gTLR.2	Total (ng)
Construct length (bp)	9551	3056	3046	3046	
DNA per well (ng)	**1327**	**423**			**1750**
	1327		**423**		**1750**
	1327			**423**	**1750**

Note: One day after transfecting the indicated plasmids, IDLV[d] particles were added at an MOI of 8 VP/cell.

Table S5. Experimental scheme corresponding to **Figure 3** (**Protocol A**)

DONOR: Plasmid[d]	3.25 ×10[5] HER.TLR[TetO.KRAB] cells per well of 24-well plates (500 µl medium per well with or without Dox)						
	PEI (1mg/ml)： 9.6 µl per well; Ratio DNA / PEI equivalents = 10						
Reagents	Cas9	gNT (Ctrl)	gTLR.1	gTLR.2	gTLR.3	Plasmid[d]	Total (ng)
Construct length (bp)	9551	3056	3046	3046	3047	6194	
DNA per well (ng)	**890**	**284**				**577**	**1751**
	890		**284**			**577**	**1751**
	890			**284**		**577**	**1751**
	890				**284**	**577**	**1751**

Note: The same transfection conditions were applied in experiments carried out in control, Dox-unresponsive, HER.TLR[KRAB] cells (**Figure 4**).

Table S6. Experimental scheme corresponding to **Figure 3** (**Protocol B**)

DONOR: Plasmid[d]	3.25 ×10[5] HER.TLR[TetO.KRAB] cells per well of 24-well plates (500 µl medium per well with or without Dox)					
	PEI (1mg/ml)： 5.8 µl per well; Ratio DNA / PEI equivalents = 6					
Reagents	Cas9	gNT (Ctrl)	gTLR.1	gTLR.2	Plasmid[d]	Total (ng)
Construct length (bp)	9551	3056	3046	3046	6194	
DNA per well (ng)	**890**	**284**			**577**	**1751**
	890		**284**		**577**	**1751**
	890			**284**	**577**	**1751**

Table S7. Experimental scheme corresponding to **Figure 6**

DONOR: Plasmid[d]		3.25 ×10[5] HER.TLR[TetO.KRAB] cells per well of 24-well plates (500 µl medium per well with or without Dox)						
		PEI (1mg/ml)： 9.6 µl per well; Ratio DNA / PEI equivalents = 10						
Reagents	Cas9	gNT (Ctrl)	gTLR.1	gTLR.2	gTLR.3	Plasmid[d]	Plasmid[S]	Total (ng)
Construct length (bp)	8506	3056	3046	3046	3047	6194	6040	
DNA per well (ng)	**823**	**295**				**599**	**33**	**1750**
	823		**295**			**599**	**33**	**1750**
	823			**295**		**599**	**33**	**1750**
	823				**295**	**599**	**33**	**1750**

DONOR: Plasmid[d]	3.25 ×10[5] HER.TLR[TetO.KRAB] cells per well of 24-well plates (500 µl medium per well with or without Dox)						
	PEI (1mg/ml)： 9.6 µl per well; Ratio DNA / PEI equivalents = 10						
Reagents	Cas9[hGem(1/110)]	gNT (Ctrl)	gTLR.1	gTLR.2	gTLR.3	Plasmid[d]	Total (ng)
Construct length (bp)	8854	3056	3046	3046	3047	6194	
DNA per well (ng)	**856**	**295**				**599**	**1751**
	856		**295**			**599**	**1751**
	856			**295**		**599**	**1751**
	856				**295**	**599**	**1751**

Notes: The source of Cas9 and Cas9[hGem(1/110)] proteins were isogenic expression plasmids pX330.Cas9 and pX330.Cas9.hGem(1/110), respectively; Plasmid[S] refers to an irrelevant ("stuffer") construct to normalize the total amount of transfected DNA; The same transfection conditions were applied in experiments carried out in control, Dox-unresponsive, HER.TLR[KRAB] cells.

Table S8. Experimental scheme corresponding to **Figure 5**

DONOR: pTHG.Donor (Exp.1)	2.0 ×10[5] HEK.EGFP[TetO.KRAB] cells per well of 24-well plates (500 µl medium per well with or without Dox)				
	PEI (1mg/ml)： 6.2 µl per well; Ratio DNA / PEI equivalents = 9				
Reagents	eCas9	gEGFP	gNT (Ctrl)	pTHG.Donor	Total (ng)
Construct length (bp)	9360	3046	3056	3561	
DNA per well (ng)	**733**	**238**		**279**	**1250**
	733		**238**	**279**	**1250**
DONOR: pTHG.Donor (Exp.2)	2.0 ×10[5] HEK.EGFP[TetO.KRAB] cells per well of 24-well plates (500 µl medium per well with or without Dox)				
	PEI (1mg/ml)： 6.2 µl per well; Ratio DNA / PEI equivalents = 9				
Reagents	eCas9	gEGFP	gNT (Ctrl)	pTHG.Donor	Total (ng)
Construct length (bp)	9403	3046	3056	3561	
DNA per well (ng)	**733**	**238**		**279**	**1250**
	733		**238**	**279**	**1250**

Table S9. Experimental scheme corresponding to **Figure S3**

DONOR: ODN.s / ODN.as	2.5×10^5 HEK.EGFP$^{TetO.KRAB}$ cells per well of 24-well plates (500 µl medium per well with or without Dox)						
	PEI (1mg/ml)： 6.2 µl per well; Ratio DNA / PEI equivalents = 9						
Reagents	Cas9	gNT (Ctrl)	gEGFP	ODN.s	ODN.as	Total (ng)	Molar ratios
Construct length (bp)	9551	3056	3046	120	120		
DNA per well (ng)	**642**	**205**		**403**		**1250**	**1:1:50**
	766		**244**	**240**		**1250**	**1:1:25**
	642		**205**	**403**		**1250**	**1:1:50**
	642	**205**			**403**	**1250**	**1:1:50**
	766		**244**		**240**	**1250**	**1:1:25**
	642		**205**		**403**	**1250**	**1:1:50**

Table S10. Experimental scheme corresponding to **Figure 7C**

DONOR: ODN.s / ODN.as	2.5×10^5 HEK.EGFP$^{TetO.KRAB}$ cells per well of 24-well plates (500 µl medium per well with or without Dox)					
	PEI (1mg/ml): 6.2 µl per well; Ratio DNA / PEI equivalents = 9					
Reagents	Cas9	gNT (Ctrl)	gEGFP	ODN.as	Total (ng)	Molar ratios
Construct length (bp)	9551	3056	3046	120		
DNA per well (ng)	**642**	**205**		**403**	**1250**	**1:1:50**
	766		**244**	**240**	**1250**	**1:1:25**
	642		**205**	**403**	**1250**	**1:1:50**
	553		**176**	**521**	**1250**	**1:1:75**

Note: The molar ratios 1:1:50 of Cas9:gRNA:oligos were used in the experiments correponsing to the flow cytometry dot plots presented in Figure 6B.

Supplementary Notes

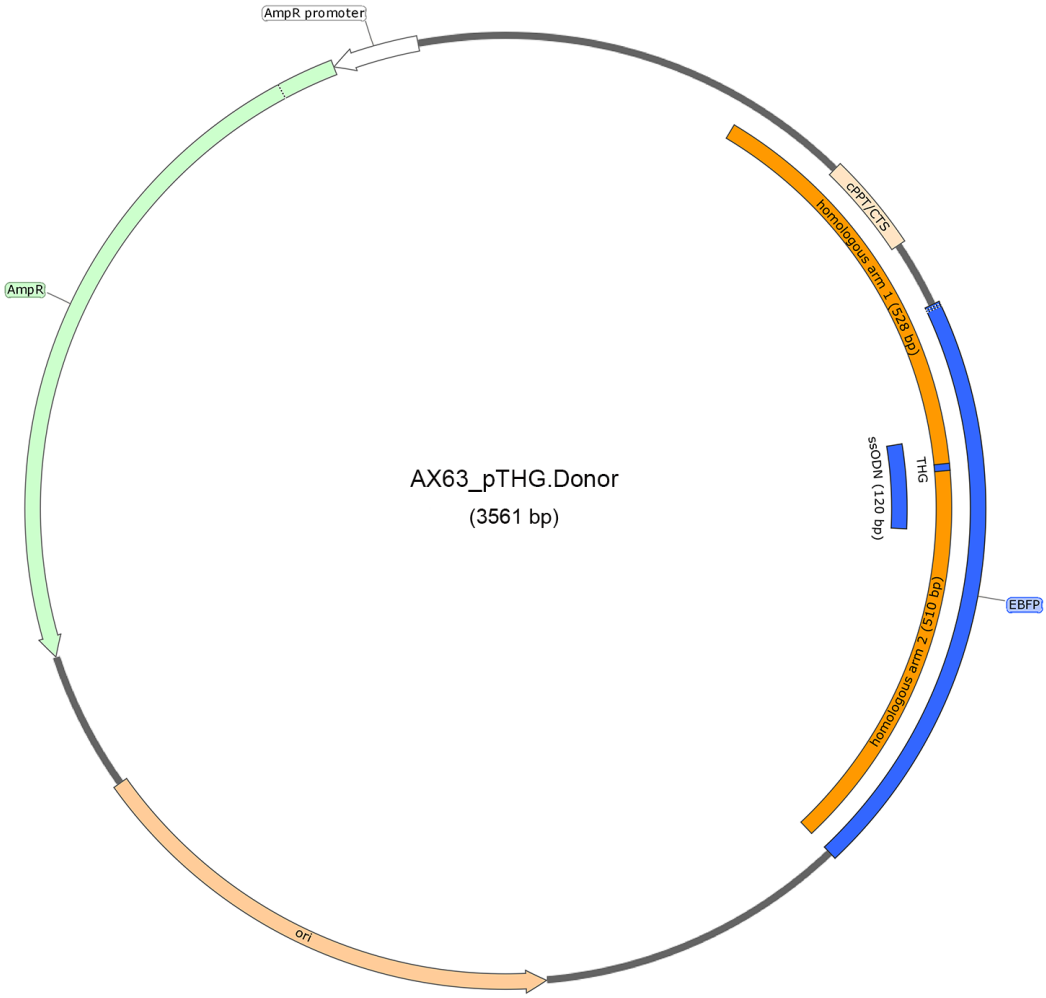

>AX63_pTHG.Donor

GGAAACAGCTATGACCATGATTACGCCAAGCTCGAAATTACCCCTCACTAAAGGGAACAAAGCTGGTACGAGGACAGGCT

GGAGCCATGGGCATGGCTACTCAAGCTGATTTGATGGAGTTGGACATGGCCATGGCTGGTGACCACGTCGTGGAATGCCT

TCGAATTCAGCACCTGCACATGGGACGTCGACCTGAGGTAATTATAACCCGGGCCCTATATATGGATCCAATTGCAATGA

TCATCATGACAGATCTGCGCGCGATCGATATCAGCGCTTTAAATTTGCGCATGCTAGCTATAGTTCTAGAGCCTCTGCTA

ACCATGTTCATGCCTTCTTCTTTTTCCTACAGCTCCTGGGCAACGTGCTGGTTATTGTGCTGTCTCATCATTTTGGCAAA

GAATTAAATTTAATTAATCTCGACGGTATCGGTTAACTTTTAAAAGAAAAGGGGGGATTGGGGGGTACAGTGCAGGGGAA

AGAATAGTAGACATAATAGCAACAGACATACAAATTTAAAGAATTACAAAAACAAATTACAAAAATTCAAAATTTTATCG

ATCACGAGACTAGCCTCGAGGTTTAAACTACGGGATCCAGGCCTAAGCTTACGCGTCCTAGCGCTACCGGTCGCCACCAT

GGTGAGCAAGGGCGAGGAGCTGTTCACCGGGGTGGTGCCCATCCTGGTCGAGCTGGACGGCGACGTAAACGGCCACAAGT

TCAGCGTGTCCGGCGAGGGCGAGGGCGATGCCACCTACGGCAAGCTGACCCTGAAGTTCATCTGCACCACCGGCAAGCTG

CCCGTGCCCTGGCCCACCCTCGTGACCACCCTGACACATGGCGTGCAGTGCTTCAGCCGCTACCCCGACCACATGAAGCA

GCACGACTTCTTCAAGTCCGCCATGCCCGAAGGCTACGTCCAGGAGCGCACCATCTTCTTCAAGGACGACGGCAACTACA

AGACCCGCGCCGAGGTGAAGTTCGAGGGCGACACCCTGGTGAACCGCATCGAGCTGAAGGGCATCGACTTCAAGGAGGAC

GGCAACATCCTGGGGCACAAGCTGGAGTACAACTACAACAGCCACAACGTCTATATCATGGCCGACAAGCAGAAGAACGG

CATCAAGGTGAACTTCAAGATCCGCCACAACATCGAGGACGGCAGCGTGCAGCTCGCCGACCACTACCAGCAGAACACCC
CCATCGGCGACGGCCCCGTGCTGCTGCCCGACAACCACTACCTGAGCACCCAGTCCGCCCTGAGCAAAGACCCCAACGAG
AAGCGCGATCACATGGTCCTGCTGGAGTTCGTGACCGCCGCCGGGATCACTCTCGGCATGGACGAGCTGTACAGAGCTCG
AGAAGTACTAGTGGCCACGTGGGCCGTGCACCTTAAGCTTTTAAATAAGGAGGAATAACATATGACCATGATTACGCCAA
GCTCCAATTCGCCCTATAGTGAGTCGTATTACAATTCACTGGCCGTCGTTTTACTATGCGGTGTGAAATACCGCACAGAT
GCGTAAGGAGAAAATACCGCATCAGGCGCTCTTCCGCTTCCTCGCTCACTGACTCGCTGCGCTCGGTCGTTCGGCTGCGG
CGAGCGGTATCAGCTCACTCAAAGGCGGTAATACGGTTATCCACAGAATCAGGGGATAACGCAGGAAAGAACATGTGAGC
AAAAGGCCAGCAAAAGGCCAGGAACCGTAAAAAGGCCGCGTTGCTGGCGTTTTTCCATAGGCTCCGCCCCCCTGACGAGC
ATCACAAAAATCGACGCTCAAGTCAGAGGTGGCGAAACCCGACAGGACTATAAAGATACCAGGCGTTTCCCCCTGGAAGC
TCCCTCGTGCGCTCTCCTGTTCCGACCCTGCCGCTTACCGGATACCTGTCCGCCTTTCTCCCTTCGGGAAGCGTGGCGCT
TTCTCATAGCTCACGCTGTAGGTATCTCAGTTCGGTGTAGGTCGTTCGCTCCAAGCTGGGCTGTGTGCACGAACCCCCCG
TTCAGCCCGACCGCTGCGCCTTATCCGGTAACTATCGTCTTGAGTCCAACCCGGTAAGACACGACTTATCGCCACTGGCA
GCAGCCACTGGTAACAGGATTAGCAGAGCGAGGTATGTAGGCGGTGCTACAGAGTTCTTGAAGTGGTGGCCTAACTACGG
CTACACTAGAAGGACAGTATTTGGTATCTGCGCTCTGCTGAAGCCAGTTACCTTCGGAAAAAGAGTTGGTAGCTCTTGAT
CCGGCAAACAAACCACCGCTGGTAGCGGTGGTTTTTTTGTTTGCAAGCAGCAGATTACGCGCAGAAAAAAAGGATCTCAA
GAAGATCCTTTGATCTTTTCTACGGGGTCTGACGCTCAGTGGAACGAAAACTCACGTTAAGGGATTTTGGTCATGAGATT
ATCAAAAAGGATCTTCACCTAGATCCTTTTAAATTAAAAATGAAGTTTTAAATCAATCTAAAGTATATATGAGTAAACTT
GGTCTGACAGTTACCAATGCTTAATCAGTGAGGCACCTATCTCAGCGATCTGTCTATTTCGTTCATCCATAGTTGCCTGA
CTCCCCGTCGTGTAGATAACTACGATACGGGAGGGCTTACCATCTGGCCCCAGTGCTGCAATGATACCGCGAGACCCACG
CTCACCGGCTCCAGATTTATCAGCAATAAACCAGCCAGCCGGAAGGGCCGAGCGCAGAAGTGGTCCTGCAACTTTATCCG
CCTCCATCCAGTCTATTAATTGTTGCCGGGAAGCTAGAGTAAGTAGTTCGCCAGTTAATAGTTTGCGCAACGTTGTTGCC
ATTGCTGCAGGCATCGTGGTGTCACGCTCGTCGTTTGGTATGGCTTCATTCAGCTCCGGTTCCCAACGATCAAGGCGAGT
TACATGATCCCCCATGTTGTGCAAAAAAGCGGTTAGCTCCTTCGGTCCTCCGATCGTTGTCAGAAGTAAGTTGGCCGCAG
TGTTATCACTCATGGTTATGGCAGCACTGCATAATTCTCTTACTGTCATGCCATCCGTAAGATGCTTTTCTGTGACTGGT
GAGTACTCAACCAAGTCATTCTGAGAATAGTGTATGCGGCGACCGAGTTGCTCTTGCCCGGCGTCAACACGGGATAATAC
CGCGCCACATAGCAGAACTTTAAAAGTGCTCATCATTGGAAAACGTTCTTCGGGGCGAAAACTCTCAAGGATCTTACCGC
TGTTGAGATCCAGTTCGATGTAACCCACTCGTGCACCCAACTGATCTTCAGCATCTTTTACTTTCACCAGCGTTTCTGGG
TGAGCAAAAACAGGAAGGCAAAATGCCGCAAAAAAGGGAATAAGGGCGACACGGAAATGTTGAATACTCATACTCTTCCT
TTTTCAATATTATTGAAGCATTTATCAGGGTTATTGTCTCATGAGCGGATACATATTTGAATGTATTTAGAAAAATAAAC
AAATAGGGGTTCCGCGCACATTTCCCCGAAAAGTGCCACCTGACGTCTAAGAAACCATTATTATCATGACATTAACCTAT
AAAAATAGGCGTATCACGAGGCCCTTTCGTCTTCAAGAATT

Map and nucleotide sequence of pTHG.Donor for HDR-mediated editing of *EGFP* into *EBFP*. DNA sequences sharing identity to the target sequence in HEK.EGFP$^{TetO.KRAB}$ cells are indicated in orange; AmpR, *β-lactamase* ampicillin resistance gene; ori, high-copy number ColE1 prokaryotic origin of replication; cPPT/CTS, central polypurine tract and central termination sequence of HIV-1. As reference, the nucleotide sequences corresponding to the EBFP flurochrome (Thr-His-Gly) and the ssODNs are highlighted in blue and underlined, respectively.